Rheology and Confocal Reflectance Microscopy as Probes of Mechanical Properties and Structure during Collagen and Collagen/Hyaluronan Self-Assembly

Ya-li Yang and Laura J. Kaufman*
Department of Chemistry, Columbia University, New York, New York 10027

ABSTRACT In this work, the gelation of three-dimensional collagen and collagen/hyaluronan (HA) composites is studied by time sweep rheology and time lapse confocal reflectance microscopy (CRM). To investigate the complementary nature of these techniques, first collagen gel formation is investigated at concentrations of 0.5, 1.0, and 1.5 mg/mL at 37°C and 32°C. The following parameters are used to describe the self-assembly process in all gels: the crossover time (t_c), the slope of the growth phase (k_g), and the arrest time (t_a). The first two measures are determined by rheology, and the third by CRM. A frequency-independent rheological measure of gelation, t_g, is also measured at 37°C. However, this quantity cannot be straightforwardly determined for gels formed at 32°C, indicating that percolation theory does not fully capture the dynamics of collagen network formation. The effects of collagen concentration and gelation temperature on k_g, t_c, and t_a as well as on the mechanical properties and structure of these gels both during gelation and at equilibrium are elucidated. Composite collagen/HA gels are also prepared, and their properties are monitored at equilibrium and during gelation at 37°C and 32°C. We show that addition of HA subtly alters mechanical properties and structure of these systems both during the gelation process and at equilibrium. This occurs in a temperature-dependent manner, with the ratio of HA deposited on collagen fibers versus that distributed homogeneously between fibers increasing with decreasing gelation temperature. In addition to providing information on collagen and collagen/HA structure and mechanical properties during gelation, this work shows new ways in which rheology and microscopy can be used complementarily to reveal details of gelation processes.

INTRODUCTION

Cells in tissues are surrounded by the complex microenvironment known as extracellular matrix (ECM), which contains biomacromolecules including collagens, glycosaminoglycans (GAGs), proteoglycans, and glycoproteins (1). Although the relative amounts of these components vary substantially across tissue types, type I collagen is the chief structural component of most mammalian tissue. Type I collagen undergoes self-assembly into fibers that are organized differently in different tissues, including as perpendicular sheets in bone and the cornea, as extensive parallel arrays in tendons and ligaments, and as isotropic structural networks in most connective tissues (2). Collagen I matrices have been used both as three dimensional (3D) in vitro approximations in which to study cell behavior and for bioengineering ends. For both types of application it is often desirable to employ collagen in conjunction with other ECM macromolecules, as doing so influences the self-assembly of collagen, which in turn affects the equilibrium structure and mechanical properties as well as the biochemical composition and function of the resulting composites (3).

In this work, we study the equilibrium and self-assembly properties of collagen and collagen/hyaluronan composites. Hyaluronan (HA) is a linear nonsulfated GAG consisting of repeated disaccharide units of glucuronic acid and *N*-acetylglucosamine (4,5). HA is present in large amounts in the vitreous humor of the eye, the synovial fluid of the joints, and brain tissue. It has extraordinary water-retaining capacity and affects the mechanical properties of the tissues it dominates (6,7). Moreover, HA plays a major role in tissue growth and remodeling through its interactions with endogenous cell receptors such as CD44 and RHAMM (8). Incorporating HA into collagen matrices allows for the construction of biomaterials of particular architecture, mechanical properties, and biological signaling capacity that better reproduce the environments of certain tissue than does collagen alone.

Although relatively few studies of the assembly of collagen/HA composites have been undertaken, the in vitro self-assembly of collagen as a function of assembly conditions including temperature, pH, and ionic strength has been well studied (9–19). Although there remains some disagreement about the earliest events in collagen fibrillogenesis, the self-assembly of collagen monomers into fibrils in vitro is generally well understood. Collagen monomers exist as triple helices that assemble into small aggregates of 5–17 molecules, and these aggregates further assemble into fibrils (30–300 nm wide), which may bundle into fibers (composed of two or more fibrils) that interconnect and interpenetrate to form a fiber network (20,21). Increase in entropy of the associated solvent ostensibly drives the self-assembly. Hydrophobic interactions can stabilize the monomer backbone, and in preparations in which the nonhelical ends of the collagen molecules are retained, covalent bonds form between the nonhelical monomer ends and helical cross-linking sites. Collagen fibrils and fibers may be stabilized

Submitted May 2, 2008, and accepted for publication October 8, 2008.

*Correspondence: kaufman@chem.columbia.edu

Editor: Elliot L. Elson.

0006-3495/09/02/1566/20 $2.00

doi: 10.1016/j.bpj.2008.10.063

with both noncovalent and covalent bonds (21). Interconnections between fibers formed in vitro are largely via entanglement, and thus, the fully developed collagen network is a complex physicochemical gel (19).

The great majority of studies that have investigated collagen fibrillogenesis have employed turbidity measurements. Early analysis of such experiments showed collagen fibril growth to be consistent with a nucleation-and-growth mechanism (9–12). This is reflected in the shape of the turbidity curves as they develop over time during gelation. These curves are generally sigmoidal and display a lag phase (nucleation) in which turbidity is unchanged, followed by a growth phase in which turbidity rapidly increases before a plateau is reached as the available collagen is depleted. The plateau value is a complicated function of fibril size, bundling, and number, as is the value of turbidity during the entirety of the growth phase. In addition to the fact that turbidity measurements cannot reveal details of fiber number and size, they also cannot sensitively reflect fibril or fiber connections (chemical or physical) that may develop late in the gelation process. Such connections have important consequences for the mechanical properties of the systems and are important considerations for bioengineering and biophysical applications of collagen-based gels. A recent study on collagen gelation tracked the development of such mechanical properties by employing rheology rather than turbidity (19). The development of the gel viscoelasticity was monitored in time via oscillatory rheology, and the development of the collagen network was found to be consistent with percolation theory of branched networks (22–26). In addition to the multitude of studies on pure collagen fibrillogenesis, several studies have investigated the structure and gelation dynamics of composite gels containing collagen and other ECM components (3,27–37). The studies in this area have shown that different GAG molecules affect collagen gelation kinetics differently. In particular, several studies have shown that HA does not significantly alter collagen gelation kinetics or fibril structure, although there is some disagreement on these points (27,33,34).

Here, we investigate the structure, mechanical properties, and gelation dynamics of collagen and collagen/HA matrices. Equilibrium structure is ascertained via scanning electron microscopy (SEM), confocal reflectance microscopy (CRM), and confocal fluorescence microscopy (CFM). Equilibrium mechanical properties are investigated via rheology. Structure during gelation is monitored by time-lapse CRM. CRM has been used to image collagen gelation previously in one study (18) and has also been used to monitor collagen during cell migration experiments (38–40). To monitor mechanical properties during gelation, time-sweep rheology studies are performed. Comparison of CRM and rheology during gelation yields new information on the structures that give rise to the mechanical properties of collagen gels during gelation as a function of collagen concentration and gelation temperature. Monitoring the equilibrium and nonequilibrium structures and mechanical properties of collagen/HA gels shows that HA can both deposit on collagen fibrils and remain dispersed throughout the matrix. The gelation temperature of collagen/HA systems affects the dynamics of collagen assembly, which in turn affects the relative amounts of deposited and dispersed HA and the composite gels' equilibrium structure and mechanical properties. This work thus yields a fuller understanding of the self-assembly behavior of collagen alone and in the presence of other ECM components at physiological conditions, which is relevant for understanding the in vivo assembly of ECM. This work also clarifies how gelation conditions lead to the development of systems of given structure and mechanical properties, which in turn will allow for enhanced rational design of biomaterials of tailored architecture, mechanical properties, biochemical composition, and molecular availability.

We first introduce the use of time-sweep rheology and time-lapse CRM for the study of collagen gelation by presenting results from these methods on pure collagen gels formed at physiological temperature at three concentrations. We then discuss, in turn, the equilibrium properties and gelation kinetics of collagen/HA matrices at 37°C, pure collagen matrices at 32°C, and collagen/HA matrices at 32°C. Formation of these networks are discussed in terms of both nucleation-and-growth and percolation theory.

MATERIALS AND METHODS

Materials

PureCol collagen (pepsin-solubilized purified sterile bovine collagen in solution) is obtained from Inamed (Fremont, CA). The solution is ~97% collagen I and 3% collagen III and is reported to be 80% monomeric, with the rest present as oligomers (41). The solution is delivered at ~3 mg/mL and pH 2. Hyaluronic acid sodium salt from rooster comb (H5388) and fluorescein-labeled hyaluronic acid (F1177) are obtained from Sigma (St. Louis, MO). HA solids are dissolved in sterile water to prepare fresh stock solution at 4 mg/mL. DMEM 10× solution and sterile NaOH (1 N) are purchased from Sigma. Gibco HEPES buffer (1 M) is obtained from Invitrogen (Carlsbad, CA). Fixation supplies necessary for SEM studies are 3% (v/v) glutaraldehyde containing 3% (w/v) paraformaldehyde, obtained from Electron Microscopy Sciences (Hatfield, PA), and dimethylsulfoxide, sodium cacodylate, and cetylpyridinium chloride, all obtained from Sigma.

Preparation of 3D collagen and collagen/HA gels

Collagen and collagen/HA gels are prepared by diluting the PureCol collagen solution and (as needed) the stock HA solution in cell culture medium. Appropriate amounts of stock solutions of collagen (3.0 mg/mL) and HA (4.0 mg/mL), depending on the final concentrations desired, are mixed at 4°C with 0.2 mL DMEM 10× solution and 50 μL HEPES buffer (1 M); 0.5 M NaOH is added to bring the pH to 7.4. Deionized water is added to bring the total volume to 2.0 mL. We prepare collagen and collagen/HA solutions with these components rather than with phosphate-buffered saline because we wish to prepare gels that are compatible with cell health. All solutions are well mixed and kept at 4°C. Gel matrices that are not gelled in situ during either rheology or microscopy are formed by incubation at 37°C or 32°C for at least 60 min.

Rheology

Rheological experiments are conducted on an AR-2000 rheometer with built-in temperature and gap calibration (TA Instruments). A 1° acrylic cone geometry (diameter 60 mm, 27 μm truncation) with a solvent trap is used. All experiments are conducted in oscillatory mode. Preliminary strain sweep tests at a fixed frequency were performed to determine the strain amplitude range of the linear viscoelastic regime. For all remaining measurements, the controlled variable is set to be strain, with stress varying to achieve a strain amplitude of 0.8% for all experiments. In all cases, 1 mL of collagen solution is neutralized and then applied to the measuring stage at 4°C. After trimming the sample according to the geometry, we added the solvent trap and elevated the temperature to 37°C or 32°C. The sample stage reaches the desired temperature within 1 min. Five seconds after this, the experiment is started. Time sweeps are performed at 37°C for 30 min and at 32°C for 60 min at fixed frequency (1 Hz) to monitor the in situ gelation dynamics of collagen and collagen/HA solutions. Storage modulus, G' (Pa), and loss modulus, G'' (Pa), are measured in each run. All tests are repeated at least three times. Several time sweeps are also performed at 0.1 Hz and 0.5 Hz to allow for definition of the gelation time, t_g, as described in Results and Discussion. Additionally, frequency sweep measurements (0.1–10 Hz) of fully developed gels are performed. For time sweep data, the rates of gelation in different systems are compared via the normalized elastic modulus, $G'_r = [G'(t) - G'_0]/[G'_\infty - G'_0]$, where G'_0 is the elastic modulus of the starting solution and G'_∞ is the equilibrium elastic modulus after complete gelation. G'_∞ is the average of the last 10 G' points obtained from a time-sweep test.

Microscopy

For structural studies, 400–500 μL of 4°C collagen or collagen/HA solution is loaded into a cylindrical chamber made from a 1-cm-diameter plexiglass cylinder of 2-cm height sealed on a thin coverslip by UV epoxy. CRM images are recorded with an inverted confocal laser scanning microscope (Olympus Fluoview) equipped with a 60×, NA = 1.42 oil objective. An Ar^+ laser at 488 nm is used to illuminate the sample, and the reflected light is detected with photomultiplier tube (PMT) detectors. Scans are 1024 × 1024 pixels, and all images are taken 80–100 μm into the samples. All CRM images are presented as collected, with no image processing. The bright spot in the center of the CRM images is an artifact commonly seen in CRM imaging caused by the reflection of one or more of the optical elements in the microscope (42).

For equilibrium structure measurements, solutions are transferred to either an incubator at 37°C or a warming box at 32°C. Images are taken after 60 min gelation for samples gelled at 37°C and for >60 min (typically between 60 and 120 min) for samples gelled at 32°C. For dynamic imaging of fibrillogenesis, after collagen or collagen/HA solution is added to the chamber, the solution is kept at room temperature for 2 min, transferred to a microscope incubator (Neue Biosciences), and kept in this incubator for 1 min before imaging. A homebuilt objective heater is used to further control the sample temperature as measured by a thermometer positioned adjacent to the sample. For dynamic imaging, two PMTs are used. One detector is set at high sensitivity to capture early fibrillogenesis events, and one is set at low sensitivity such that final gel images have few saturated pixels. Scans are collected at 3.26 s per scan, and the time interval between imaged slices is 30 s. The total recording time is either 20 or 30 min. To image fluorescein-labeled HA via CFM, a dichroic mirror and a long-pass 510-nm filter are used. These ensure rejection of all reflected light at 488 nm.

SEM

Collagen and collagen/HA solutions are incubated at 37°C or 32°C for at least 60 min. The gels are then fixed in 3% (v/v) glutaraldehyde containing 3% (w/v) paraformaldehyde and 2.5% (v/v) dimethylsulfoxide in 0.1 M sodium cacodylate buffer (pH 7.4) for at least 12 h at room temperature. Cetylpyridinium chloride (1%, w/v) is added to the second fixative to prevent loss of HA (30). Gels are washed extensively with 0.1 M sodium cacodylate buffer (pH 7.4), dehydrated in a graded series of ethanol solutions (50%, 75%, 90%, 95%, 100% × 3, 10 min in each) and critical-point dried from ethanol in CO_2. The dried gels are mounted on the SEM stub with silver conducting adhesive, sputter-coated with 10-nm gold-platinum, and examined in a Hitachi 4700 scanning electron microscope at 10 kV at 4000× and 20,000× magnification.

Image analysis

To quantify fibril diameter from SEM images, fibrils are manually measured using the line-drawing feature of NIH Image J. Images of several regions of at least one sample are taken, and at least 200 fibrils are measured in each case. Mean and standard deviation are reported.

For CRM images, mesh size, fiber number, and average fiber length are quantified. To measure these quantities, the CRM artifact is first removed from the images. The central portion of the image with reflectance of an intensity similar to that of collagen fibers (typically, 100 × 100 pixels) is replaced by a copy of the upper left hand corner of the image, so that representative fibers and fiber spacings are present throughout the image. The images are then thresholded. The threshold is determined by comparing the intensities of the brightest background pixels to the dimmest fiber pixels, with ''background'' and ''fiber'' pixels being differentiated through visual inspection. For mesh size determination, the threshold is chosen to remove as much noise as possible while retaining fiber pixels. Mesh size determination is then performed as described by Kaufman et al. (39). Briefly, distances between pixels above threshold are counted in each row and each column of an image. The distribution of mesh sizes in a given image is plotted, and a characteristic mesh size is extracted by fitting the distribution to the function $Ae^{-\beta x}$, with x the distance in micrometers and $1/\beta$ the characteristic mesh size reported. Characteristic mesh size is calculated from four images on four samples at equilibrium and three at arrest. Mean and standard deviation are reported.

To determine fiber number and fiber length, a fiber-finding algorithm similar to that described by Guo and Kaufman (43) is employed. First, thresholding is performed. The threshold is set lower than for mesh size determination because in the fiber-finding algorithm isolated background noise does not significantly affect results, whereas spurious gaps within fibers do. All pixels below threshold are set to zero. Fiber detection is performed by tracing out single fibers of defined width, W = 1–3 pixels, in a stepwise manner. First, the starting point of a fiber is identified by assessing the portion of its neighboring on-pixels in an area defined by the fiber width. Once the portion of on-pixels around a given pixel reaches a threshold value (generally, 50%), the first step of the fiber detection begins. The total intensity of surrounding pixel sets of area S as a function of angular direction is assessed. The size of the region, S, is $W \times SL$ with SL the step length, generally set to 10 pixels. If the brightest set of pixels so identified has on-pixels above the threshold, the next step continues within a certain angular range (generally 90°) around the direction of the current step. Steps continue until no pixel sets above threshold are found within the searched area, and the fiber is assumed to end. The pixels in the found fiber are set to zero before a search is done for additional fibers. The shortest fibers identified are $2SL = 20$ pixels (4.6 μm). This prevents erroneous association of nearby noise into fibers. After the fiber-finding algorithm has been performed, number of fibers and fiber length distribution are reported. Fiber length is quantified by fitting the distribution to an exponential decay and extracting a characteristic length, as for mesh size, as well as by taking the mean fiber length. In all cases, results are similar for both methods, and we report mean length. Fiber number and mean length are averaged for four samples at equilibrium and three at arrest.

RESULTS AND DISCUSSION

Collagen matrices of different concentration assembled at 37°C

Here, we demonstrate how rheology and CRM can be used complementarily to elucidate the manner in which collagen self-assembles into a network at physiological temperature.

Rheology

Gel solution is made as described in Materials and Methods. The solutions are neutralized at 4°C, and self-assembly is then initiated by raising the temperature from 4°C to 37°C. Gelation kinetics is monitored by rheology, measuring the storage modulus (G') and the loss modulus (G'') as a function of time during gelation. The value of G' reflects energy stored elastically in the system, whereas the value of G'' reflects energy dissipated through viscous effects. Fig. 1 *a* shows the evolution of G' and G'' measured at 1 Hz at 37°C at collagen concentrations of 0.5, 1.0, and 1.5 mg/mL. Initially $G'' > G'$, and both are very small, <0.1 Pa, consistent with a precursor sol solution. Both moduli increase rapidly as the self-assembly progresses. The rate of increase of G' is greater than that of the G'', which leads to a crossover of G' and G''. Such a crossover is a typical phenomenon in curing and cross-linking reactions and is referred to as the crossover point, t_c, with the crossover value $G'_c = G'(t_c) = G''(t_c)$ (44,45).

Our rheological measurements at 37°C are broadly consistent with the two-step nucleation-and-growth model of collagen fibrillogenesis. Each set of G' and G'' curves shown in Fig. 1 *a* displays a short-lived lag phase in which G' and G'' change very little, a growth phase in which G' and G'' increase quickly and during which t_c occurs, and a plateau phase, in which G' and G'' reach their equilibrium values. Assuming a two-step model of fibrillogenesis, the lag phase seen in rheology would be dominated by the formation of nuclei and potentially somewhat larger structures such as microfibrils that do not appreciably change the viscoelasticity of the solution. The growth phase would then be dominated by the growth and interconnection of such structures. We note that the rapid increase in G' probes somewhat different phenomena than does the rapid increase in turbidity that occurs during the growth phase, as G' reports on the system's ability to store elastic energy rather than to scatter light. A system composed of large, unconnected clusters, for example, may have little ability to store elastic energy yet have substantial turbidity. Thus, we would expect the growth phase as measured by rheology to be at least as long as the growth phase measured by turbidity under identical conditions. Once the equilibrium values of G' and G'' are reached, it is assumed the development of the fiber network is complete. Fig. 1 *a* and Table 1 reveal that the equilibrium elastic modulus, G'_∞, increases substantially as a function of collagen concentration, as discussed further below. Additionally, $G'_\infty \approx 10\ G''_\infty$ in all three collagen gels, consistent with other rheological measurements of collagen networks (19,31,46,47). To assist in the comparison of the gelation kinetics of the collagen solutions of different concentration measured here, $G'_r = [G'(t) - G'_0]/[G'_\infty - G'_0]$ is plotted against time (Fig. 1 *b*). Gelation rates can be compared via lag time, t_{lag}, and the slope of the curve during the growth phase, k_g. k_g is fit over the linear regime of $\log(G'_r)$, and t_{lag} is defined as the time at which that linear regime begins.

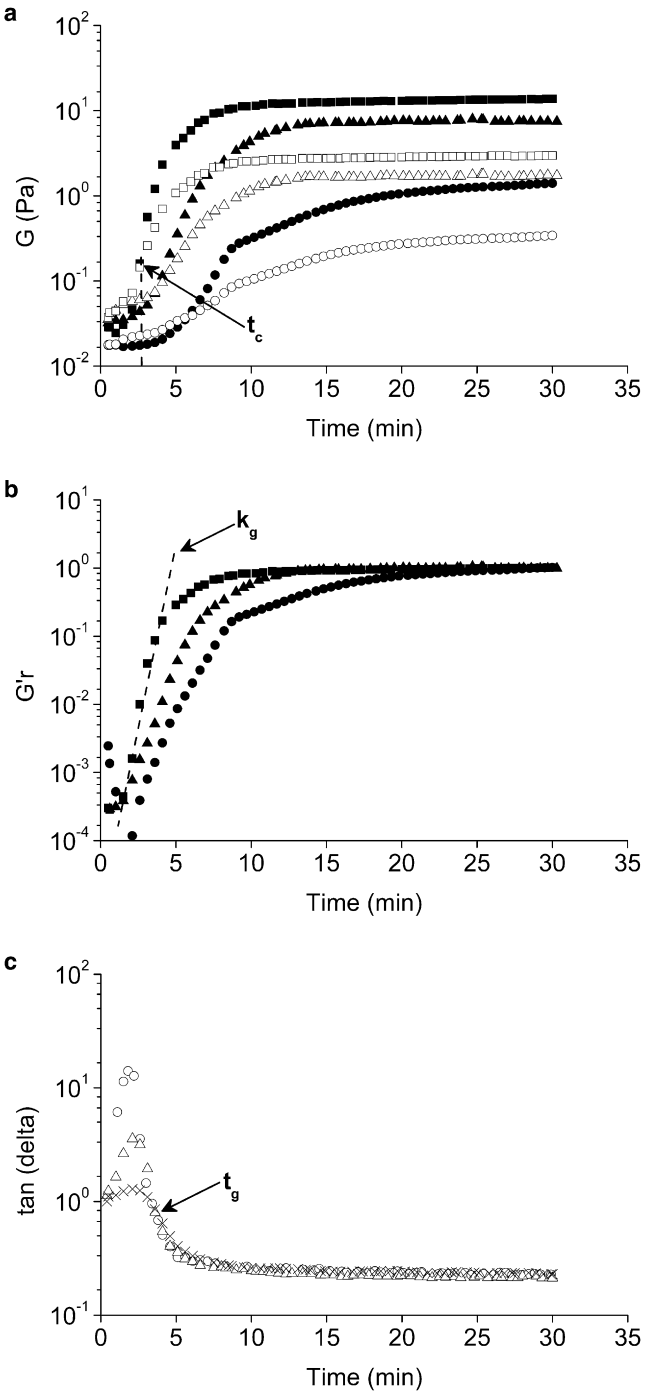

FIGURE 1 Gelation dynamics of collagen gels at 37°C as measured by rheology. (*a*) Oscillatory time sweeps at 1 Hz during gelation. Solid symbols indicate storage modulus G', and open symbols indicate loss modulus G''. Collagen concentrations are 0.5 (*circles*), 1.0 (*triangles*), and 1.5 mg/mL (*squares*). The crossover time, t_c, described in the text is indicated on the set of 1.5 mg/mL curves. (*b*) The reduced elastic modulus, G'_r, for these collagen gels. Collagen concentrations are 0.5 (*circles*), 1.0 (*triangles*), and 1.5 mg/mL (*squares*). The approximate range over which k_g is fit is indicated on the 1.5 mg/mL curve. (*c*) Loss tangent of the 1 mg/mL collagen gel with time sweeps conducted at 0.1 (*circles*), 0.5 (*triangles*), and 1.0 Hz (*crosses*). t_g is indicated.

TABLE 1 Measures of collagen and collagen/HA mechanical properties, structure, and gelation dynamics at 37°C

		Equilibrium	Dynamics			
			Rheology			CRM
			Gelation rate	Sol-gel transition		
Collagen (mg/mL)	HA (mg/mL)	G'_∞ (Pa)	k_{growth} (min^{-1} ± SD)	t_a (min ± SD)	t_g (min)/Δ	t_a (min ± SD)
0.5	0	1.39 ± 0.01	0.45 ± 0.01	5.3 ± 0.8	5.8/0.50	9 ± 2
1.0	0	7.60 ± 0.07	0.56 ± 0.01	3.9 ± 0.3	3.6/0.45	7 ± 2
1.5	0	13.14 ± 0.04	1.0 ± 0.2	2.7 ± 0.8	2.6/0.53	6 ± 1
0.5	1.8	1.79 ± 0.02	0.4 ± 0.04	10 ± 1	6.1/0.74	5.7 ± 0.3
1.0	1.8	7.95 ± 0.05	0.76 ± 0.03	5.8 ± 0.8	3.3/0.78	5.0 ± 0.5
1.5	1.2	13.3 ± 0.2	1.1 ± 0.2	3.2 ± 0.8	2.6/0.72	4.5 ± 0.5

Measures of mechanical properties (G'_∞), kinetics of gelation (k_g), and sol-gel transition (t_c, t_g, Δ, and t_a) for networks constructed at 37°C as described in the text. G'_∞ is determined from time-sweep rheology measurements at 1 Hz. The last 10 points of the rheological measurements carried out for 30 min are averaged to give G'_∞ for a particular sample. Measurements are performed on at least three samples of each type, and mean and standard deviation are presented. k_g and t_c are determined from the same time-sweep rheology measurements from which G'_∞ is obtained. k_g is found by least-squares fitting of the linear portion of $\log(G')$ versus t, as displayed in Fig. 1 *b*. t_c is the first point measured in time-sweep rheology in which $G' \geq G''$, as shown in Fig. 1 *a*. Mean and standard deviation of k_g and t_c are reported. Time-sweep rheology measurements at 0.1, 0.5, and 1.0 Hz are performed once on a set of three samples prepared at the same time. t_g is the time at which tan δ is identical for the single set of rheology time sweeps at those three frequencies, as shown in Fig. 1 *c*. Because not all samples display a fully frequency-independent crossover time, in several cases t_g is determined by the crossing of 0.1- and 1-Hz curves rather than all three. Δ is determined from the relation, $\delta_g = \Delta\pi/2$. CRM measurements such as that shown in Fig. 2 are performed on at least three different samples of each type represented in the table. Mean and standard deviation of the arrest time, t_a, are reported.

Although t_{lag} occurs very early in all the experiments presented in this work, it is evident from Fig. 1, *a* and *b*, that t_{lag} decreases as collagen concentration increases. Additionally, k_g increases as collagen concentration increases, as shown in Table 1. This acceleration of the lag and growth phases with concentration is consistent with previous results as measured via turbidity and in accord with the nucleation-and-growth model of collagen assembly (9).

In addition to differences in t_{lag} and k_g, which describe the kinetics of gelation, rheology also reveals a trend in the sol-gel transition time as a function of collagen concentration. During the growth phase, G' increases faster than G'', leading to the crossover time, t_c. At t_c, for the given frequency at which the value is determined, the mixture experiences a transition from liquid-like behavior to solid-like behavior, as defined by the presence of an elastic response at least as significant as the viscous response. Fig. 1 *a* and Table 1 show that t_c occurs earlier as a function of concentration, and G'_c is an order of magnitude higher in the 1.5 mg/mL collagen gel than in the 0.5 mg/mL gel. A frequency-independent measurement of gelation time, t_g, was also investigated, as shown in Fig. 1 *c*. The gelation time, t_g, is determined by the intersection of curves of the loss tangent ($\tan\delta = G''/G'$) versus time at several frequencies (26,45,48–50). Although this relation was originally derived for chemical gelation proceeding only through cross-linking, it has been applied with varying degrees of success to other types of gelling systems as well (19,26,51–58). The presence of such a frequency-independent crossover time, t_g, and accompanying behavior $G'(\omega) \propto G''(\omega) \propto \omega^{\Delta}$ at the gelation point is a feature of gelation proceeding through percolation and is indicative of the presence of a self-similar critical gel at that time (50,59). From t_g we can also determine Δ, as the loss tangent at t_g can be expressed as $\tan\delta_g = \tan(\Delta\pi/2)$ (48). From this relation, we find $\Delta \approx 0.5$ for collagen gelation at 37°C (Table 1). This value is below the value predicted by either analogy to electrical circuits ($\Delta = 0.72$) or Rouse theory ($\Delta = 0.67$) (60,61). However, values of $\Delta \approx 0.5$ have been seen in other systems (45,62) including the physical gel, gelatin (51). Our measured value is lower than the value of $\Delta = 0.7$ measured by Forgacs et al. for collagen solutions gelled at 12°C (19) and often reported for chemical gels (22,61). This discrepancy may result from differences in the weighting of cross-links relative to entanglements in the development of networks formed at different temperatures and/or from differently extracted monomeric collagen (63–66). We note that for systems with a value of $\Delta \approx 0.5$, t_c must be close to t_g, as it is for our collagen solutions gelled at 37°C. In all three collagen gels formed at 37°C, t_g occurs very early in the growth phase, just as G' begins to rise. Because collagen forms a network in vitro in which stiff fibers grow in length and entangle on overlapping timescales, as discussed further below, we suggest that most of this growth and entanglement, which must be the source of the rapid increase seen in G', occurs after t_g. Thus, we believe that branched network percolation theory as originally proposed for cross-linking chemical gels does not fully capture the gelation characteristics of this complex physicochemical system.

Microscopy

To interrogate the equilibrium gel structure as well as to relate the evolution of the viscoelasticity as probed by rheology to the large-scale structure of collagen gels, time-lapse CRM is performed. The gelation dynamics of a pure 1.0 mg/mL collagen solution as revealed by CRM is shown in Fig. 2 and Movie S1 in the Supporting Material. Initially,

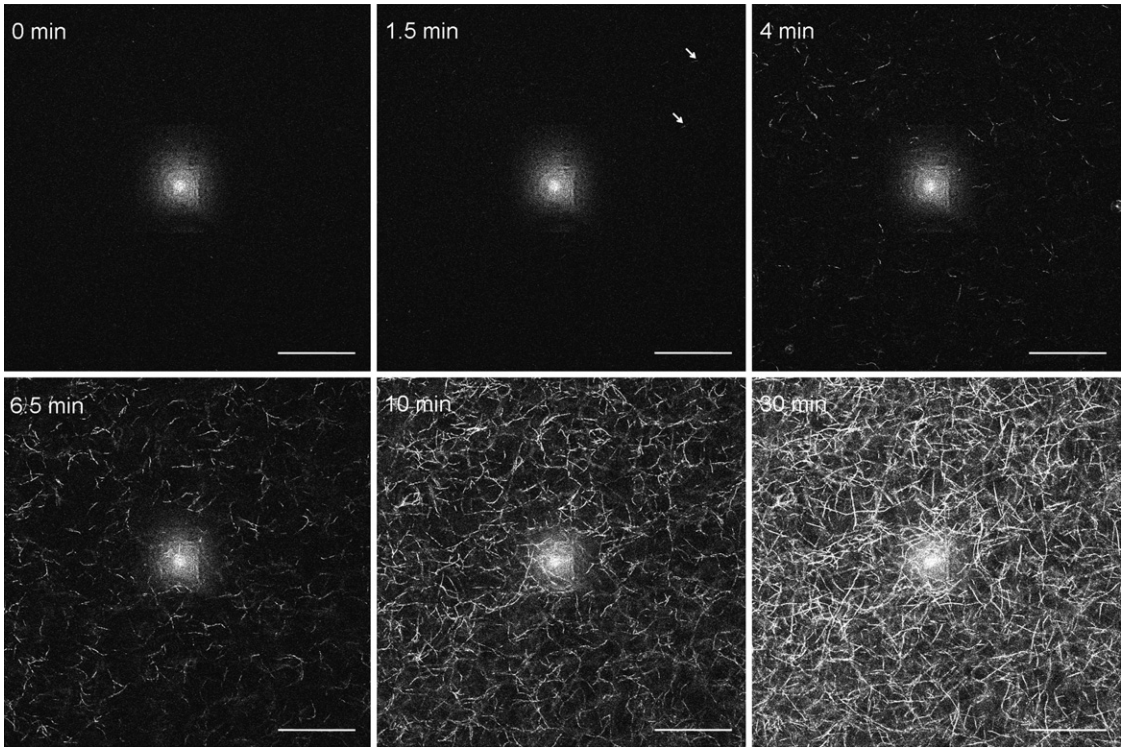

FIGURE 2 Time-lapse confocal reflectance images of collagen (1.0 mg/mL) during gelation at 37°C. Initially, no structures are resolved. At 1.5 min, the first fibers can be seen. Arrows point to two such fibers. By 4 min, many short fibers and small clusters of a few fibers can be seen. At 6.5 min, more individual fibers are visible, as are clusters of fibers. This is the arrest time (t_a) of this particular gel. At 10 min, more fibers are present. They are also clearly longer than at t_a, and many fiber interconnections are evident. The structure of the gel at the end of the imaging experiment (30 min) is also shown. Scale bar is 50 μm. As for all CRM images shown, raw data are presented. The bright spot in the center of the images is caused by reflection off optical elements in the microscope.

no structures are resolved (Fig. 2, 0 min). This is as expected because the fibrillogenesis starts from a solution of collagen monomers. After several minutes, short fibers or small clusters of a few fibers can be seen (Fig. 2, 4 min). They are randomly distributed and do not associate with each other. At this time, the sample is sol-like, and motion of fibers relative to one another can be observed. As gelation progresses, more single fibers can be seen, and the visualized fibers become longer and thicker. Simultaneously, larger clusters form. The fibers become longer at both ends and encounter other similar fibers. At some time, the fibers and clusters interconnect to form a stable immobile network. At this point the fibers abruptly stop moving relative to one another (Fig. 2, 6.5 min). It is believed this is the time the gel first spans the sample, and we term this the arrest time, t_a. Because the time-lapse imaging is done such that a two-dimensional slice of the 3D sample is visualized, the fibers seen in one slice at this time are not obviously completely connected. We expect they are connected to out-of-plane fibers. After arrest, visualized fibers continue to grow wider, perhaps reflecting fibril bundling. Additionally, fibers continue to lengthen, and further interconnections between fibers and clusters continue to form. New fibers are visualized as well, although most of the fibers that appear late in gelation are thickening fibers outside the focal plane that scatter into the plane as they grow thicker. By 30 min after the beginning of fibrillogenesis, it appears that the gel is at or very close to its equilibrium state, which is consistent with the fact that the plateau values of G' and G'' are also reached within 30 min for gelation at 37°C. Like the rheology measurements, in situ CRM imaging during collagen fibrillogenesis is broadly in accord with the two-step nucleation-and-growth model of collagen assembly. During the earliest steps of the self-assembly process, the system consists of monomers and small aggregates that cannot be visualized with CRM. By the time fibers are visualized, the growth phase has begun, and some time after the arrest time the equilibrium structure is obtained.

Structure during gelation and at equilibrium varies as a function of concentration. In general, higher-concentration gels have more fibers at all times. First, we compare structure at equilibrium (Fig. 3). We quantify the network structure as a function of concentration at equilibrium by comparing mesh size, fiber number, fiber length, and fiber width. As described in Materials and Methods, the determination of fiber number and width depends on accurate identification of fibers in the CRM images. Fig. 3, *d* and *e*, shows fibers identified in Fig. 3, *a* and *c*, to demonstrate the algorithm's ability to identify fibers in both relatively sparse and crowded collagen matrices. Careful examination of Fig. 3 *e* reveals

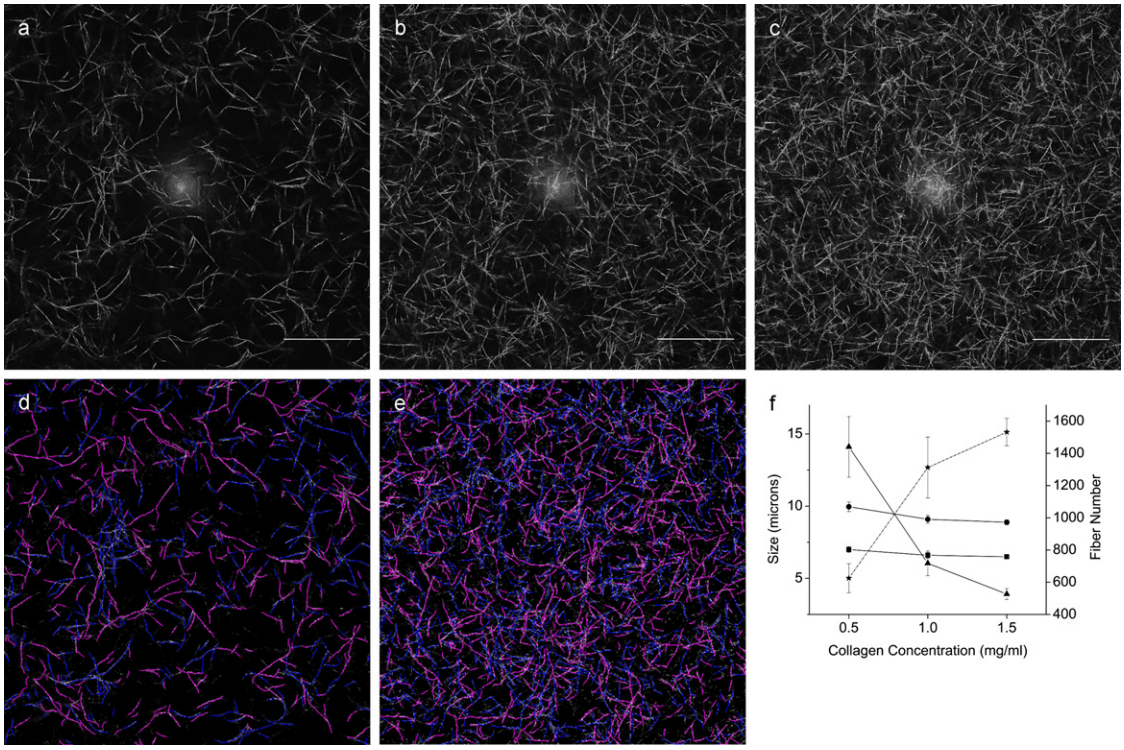

FIGURE 3 Confocal reflectance images of collagen matrices recorded after gelation for 60 min at 37°C: (*a*) 0.5 mg/mL collagen, (b) 1.0 mg/mL collagen, and (c) 1.5 mg/mL collagen. Scale bar is 50 μm. (*d*) Fibers identified with the fiber-finding algorithm described in the text and employed on the 0.5 mg/mL collagen image shown in *a*. The found fibers are drawn atop the grayscale CRM image. (*e*) Fibers identified by the fiber-finding algorithm and drawn atop the 1.5 mg/mL image shown in *c*. (*f*) Fibril diameter (×100) (■, *left axis*), fiber length (●, *left axis*), mesh size (▲, *left axis*), and number of fibers (★, *right axis*) as described in text and averaged over four images of four samples including those pictured in *a–c*.

that the least intensely reflecting fibers are not identified. This may lead to an underestimation of fiber number. Additionally, because of the high density of fiber crossings at high collagen concentration, the algorithm may erroneously connect individual fibers. This would simultaneously result in an underestimation of fiber number and an overestimation of average fiber length. Although such systematic errors likely occur to a certain extent, based on visual inspection of original images and images with identified fibers, we believe the algorithm is sufficiently robust to accurately report trends in fiber number and length.

Fig. 3 *f* summarizes findings on fiber number, length, width, and mesh size as a function of collagen concentration. (These data are also presented in comparison to other gels investigated; see Fig. 15). Fiber number increases, and mesh size decreases, with concentration. Average fiber length decreases slightly with increasing concentration. We quantify fiber width with SEM measurements on fixed collagen gels rather than confocal measurements because fiber width is expected to be on the order of optical wavelengths and no more than several pixels across in our CRM measurements. Although SEM preparation shrinks the gel and potentially the fibrils, trends in fibril diameter across collagen preparations are the same in SEM and optical microscopy (67). Fibril diameter is found to decrease slightly with concentration for collagen gels formed at 37°C. This is consistent with findings that fibril diameter is set during the nucleation phase by the shape of nuclei, which is not expected to depend strongly on concentration (10,68). On the other hand, the number of collagen fibers is expected to depend strongly on concentration. Nucleation-and-growth theory predicts $dn/dt = kC^x$, with C the collagen concentration, n the concentration of nuclei, x a constant >1 representing the number of monomers in a nucleus, and k the rate constant (10). This equation applies to the lag (nucleation) phase only, which precedes the growth phase. Although not all nuclei will grow into individual (or individually distinguishable) fibers, the total number of nuclei and thus the concentration, is expected to have a strong effect on total number of fibers present at the end of gelation.

Because fiber width and number are expected largely to be set by the shape and number of nuclei, each of which is set early in the gelation process, we expect the structure of the collagen gels at arrest to mirror that at equilibrium. Fig. 4 shows that at t_a there are more and shorter fibers as a function of increasing collagen concentration. (see Fig. 16 for a summary of the quantified variables in these gels as compared to those of other gels at arrest). In the limit of identical fiber and network structure, an identical number of collagen fibers would be expected to lead to arrest regardless

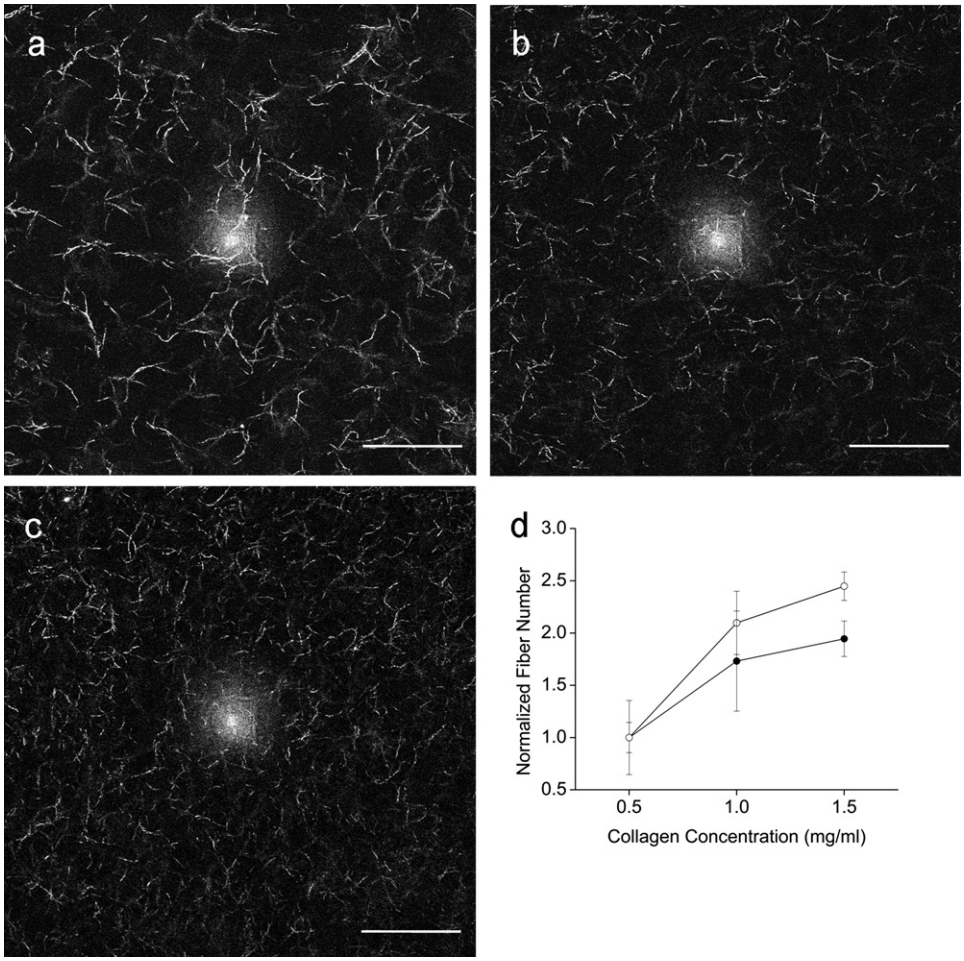

FIGURE 4 Confocal reflectance images of collagen matrices recorded at the arrest time during gelation at 37°C: (*a*) 0.5 mg/mL collagen, (*b*) 1.0 mg/mL collagen, and (*c*) 1.5 mg/mL collagen. Scale bar is 50 μm. (*d*) Normalized fiber number at arrest (●) and equilibrium (○) averaged over three images of three samples at arrest and four at equilibrium.

of concentration. Differences in fiber length and width as a function of concentration prevent that from being the case in this set of gels; however, the fact that fiber number increases more quickly with concentration at equilibrium than at arrest (Fig. 4 *d*) is consistent with the identification of the arrest time as the time at which the network spans the sample. In addition to differences in structure as a function of concentration at arrest, the time to arrest is also different. The fibers comprising the 1.5 mg/mL system at arrest form more quickly than do the fibers comprising the 0.5 mg/mL system at arrest. This can be more fully understood through comparison of CRM and rheology results.

Comparison of rheology and CRM results

As mentioned previously, a recent study used rheology to describe collagen gelation in terms of branched-network percolation (19). These authors also used phase contrast microscopy to supplement their study of collagen gelation at 1.7 mg/mL and 12°C. The microscopy in this rheological study found a similar structural progression to that which we visualize with CRM, with collagen fibers becoming visible before forming clusters that encounter one another and eventually form a network. Although our work is largely consistent with the findings of that study, we wish to more fully compare rheology and microscopy measurements to elucidate the development of network structural and mechanical properties during gelation.

First, we compare equilibrium structure with mechanical properties as revealed by CRM and rheology. The equilibrium structure and mechanical properties of the collagen gels can be correlated by comparing their structure and values of G'_∞. Over the (very limited) concentration range investigated, $G'_\infty(c) \propto c^{2.1}$. This behavior is similar to that recently found by Stein et al. over a wider concentration range (69). The increase of elastic modulus with concentration is in part driven by the increased structural protein present in the higher concentration gels and in part related to the gel structure. As collagen concentration increases, so too does the number of fibers and fiber crossings that substantially affect the mechanical properties of the system (69).

Because rheology and microscopy experiments are not performed on the same samples at the same time, direct comparison of mechanical properties as measured by rheology and structure as measured by CRM at particular times during gelation is difficult. Indeed, there are several reasons why the dynamics as measured by CRM may not be

identical to that measured by rheology. First, although all samples are prepared and kept at 4°C before gelation, those measured by rheology are typically held at 4°C after neutralization longer than those subjected to CRM, and it has been shown that there are subtle changes to collagen solutions even at 4°C (19,70). Second, the temperature of the microscope incubator is not as well controlled or homogeneous as is that of the rheometer. Third, the stress imposed by rheology may affect the gel formation, particularly at very early times during the process. Similarly, the flow field present in CRM as a result of convection and/or slight skew of the sample on the microscope stage may affect gelation. Finally, differences in sample thickness and potential number of nucleation sites on the sample container walls may affect nucleation rates. Even given these potential systematic errors, we believe qualitative comparison of gelation as measured by microscopy and rheology is useful, as is comparing trends in gelation as measured by the two techniques.

As mentioned, the same structural characteristics present in collagen gels of different concentrations at equilibrium are also present at arrest. The fibers in the 1.5 mg/mL collagen gel are more numerous and shorter than are those of the 0.5 mg/mL gel. Moreover, arrest occurs earlier in the higher-concentration gel, and the fibers that lead to arrest in the 1.5 mg/mL gel form more quickly than do the fibers that form in the lower-concentration gels. This is consistent with the earlier t_{lag} and increased k_g seen in rheology (Fig. 1 and Table 1). Additionally, we compare gelation time as measured by rheology and CRM. Table 1 shows that t_c, t_g, and t_a all become earlier as a function of collagen concentration. Despite the fact that all three times are measures of gelation, they are not identical, and the differences among these times highlight the differences between and complementary natures of rheology and CRM for the study of gelation. although t_c, t_g, and t_a all occur after the nucleation phase and during the rapid increase in G' and G'', they occur at different points within this growth phase. By the time of sol-gel transition, t_g, the system has an elastic modulus at least as great as the viscous modulus at all the frequencies measured (0.1, 0.5, and 1 Hz), indicating the formation of structures that can bear stress. For collagen gelation at 37°C, t_g and t_c report on the lag phase and the early growth phase, whereas t_a reports on the lag phase plus a significant portion of the growth phase. Isolating the kinetics of the growth phase is accomplished by measuring k_g. As discussed above, k_g increases as a function of collagen concentration, consistent with the decrease of t_a.

Collagen/HA matrices assembled at 37°C

We next discuss the equilibrium structure and mechanical properties as well as the gelation dynamics of collagen/HA systems. Although collagen fibrillogenesis has been studied in the presence of a large number of other ECM components, relatively few studies have been performed on collagen/HA composites. This is in part because an early study found that HA affects collagen fibrillogenesis more subtly than do other macromolecules such as chondroitin sulfate and heparin (27). More recent studies report conflicting data, with one recent study showing that high concentrations of low- and high-molecular-weight HA slow collagen gelation (33) and another showing an acceleration of both the lag and growth phases of collagen fibrillogenesis in the presence of HA (34). These studies also disagree on the effect of HA on fibril diameter. The relative ratio of collagen to HA as well as HA source and fibrillogenesis conditions (pH, temperature, and ionic strength) may account for such differences. Despite these differences, all studies show that collagen fibrils formed in the presence of HA have native banding, indicating that the equilibrium structure of collagen fibrils is largely unperturbed by the presence of HA. We prepare several composite collagen/HA matrices. At the collagen and HA concentrations investigated here, the composite matrices exhibit qualitatively similar equilibrium structures, mechanical properties, and gelation dynamics to pure collagen matrices of the same collagen concentration. However, details of both equilibrium properties and gelation dynamics, and in particular structure during gelation, differ with addition of HA.

Equilibrium

Fluorescein-labeled HA was used in CFM to directly determine the location of HA in collagen/HA composite gels. Consecutively collected CRM of the collagen (Fig. 5 *a*) and CFM of the HA (Fig. 5 *b*) in collagen/HA gels allows direct observation of both components. Fig. 5 shows that HA deposits along collagen fibers as is indicated by structures in CFM colocalized with collagen fibers visualized by CRM. Because all work interrogating the banding of collagen fibrils formed in the presence of HA shows native structure, and HA is expected to have weak electrostatic interactions with collagen, we believe that the deposited HA molecules are on the surface of collagen fibrils rather than intercalated into them. HA also distributes throughout the matrix, as is demonstrated by the brightness of the background in the CFM image relative to the CRM image. Control experiments with collagen and unlabeled HA employing the same detector settings show no signal in the CFM channel. Although some work suggests that in vitro HA coats collagen fibers, whereas in vivo HA molecules are dispersed within the interfibrillar space of collagen (33,71), we find that HA exists both colocalized with collagen fibers and in the interfibrillar space in our in vitro assembled collagen/HA gels. It is thus reasonable to consider that both forms of HA, the deposited HA and the dispersed HA, affect the equilibrium and nonequilibrium mechanical properties of these gels.

Quantititative image analysis of collagen/HA gels at equilibrium (Fig. 6) show that the number of collagen fibers in the presence of HA is slightly higher, and the fibers are slightly shorter, than in the absence of HA (see Fig. 15 for a summary of these data). SEM measurements of fibril diameter (Fig. 7) show that the addition of HA to collagen decreases the

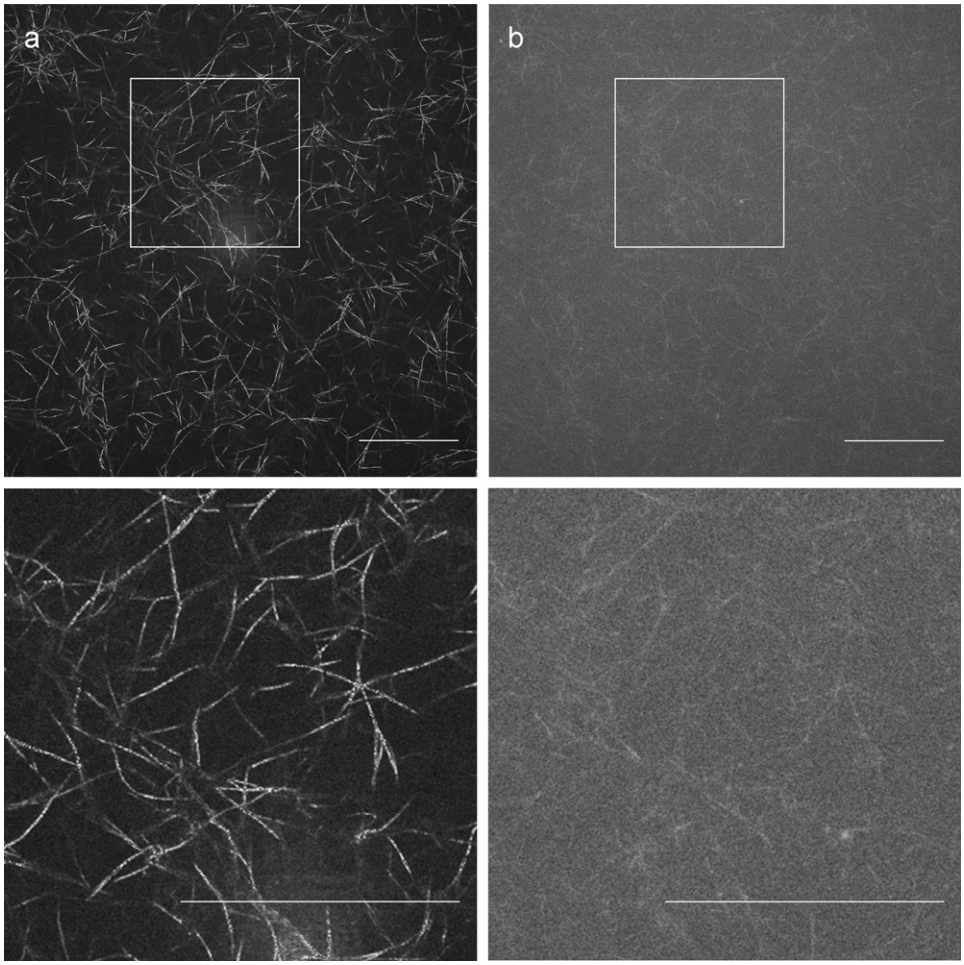

FIGURE 5 Consecutively collected (*a*) CRM and (*b*) CFM images of a 1.0 mg/mL collagen gel containing 1.8 mg/mL fluorescein-labeled HA gelled at 37°C. Lower panel shows close-ups of the squared portions of images in the upper panel. HA deposits along collagen fibers indicated by fiber structures in CFM and also distributed throughout the matrix as shown by the brightness of the background in the CFM image relative to the CRM image. Scale bar is 50 μm.

collagen fibril thickness at all concentrations. This suggests that HA changes the shape of the collagen nucleation centers. Although images presented in Fig. 7 show areas in which single fibrils are dominant, the gels are heterogeneous, and some gels have regions with substantial fibril bundling. Collagen gels with HA show less fibril bundling than gels at the same collagen concentration without HA, implying that HA inhibits lateral fusion of collagen fibrils into fibers, as has been seen in collagen/decorin composites (35). Fig. 7, *b* and *c*, also show globules present on the collagen fibrils, as electron microscopy has revealed in other studies of collagen/HA systems (30,31,33). We suggest that these globules result from the condensation of the dispersed HA, as such deposition has been seen to occur in the presence of the fixative used here, whereas a different fixation procedure showed the presence of HA fibrils of 1.5–3 nm (30).

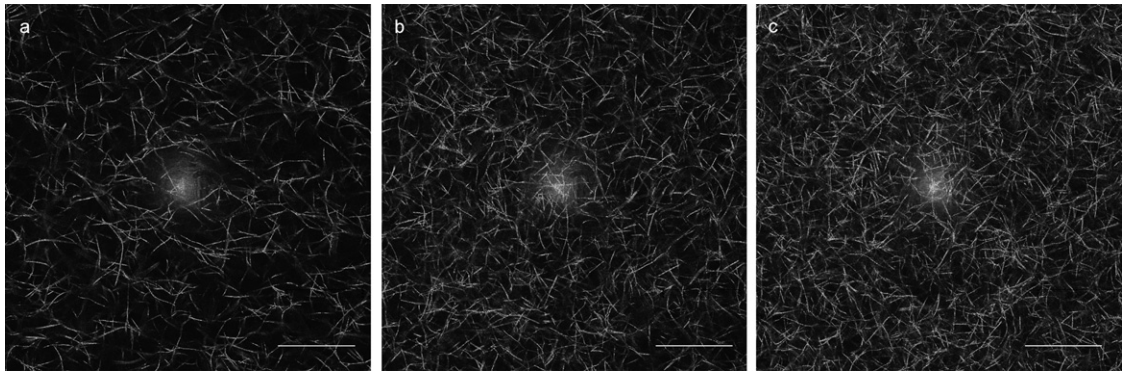

FIGURE 6 Confocal reflectance images of collagen/HA matrices recorded after gelation for 60 min at 37°C: (*a*) 0.5 mg/mL collagen and 1.8 mg/mL HA, (*b*) 1.0 mg/mL collagen and 1.8 mg/mL HA, and (*c*) 1.5 mg/mL collagen and 1.2 mg/mL HA. Scale bar is 50 μm.

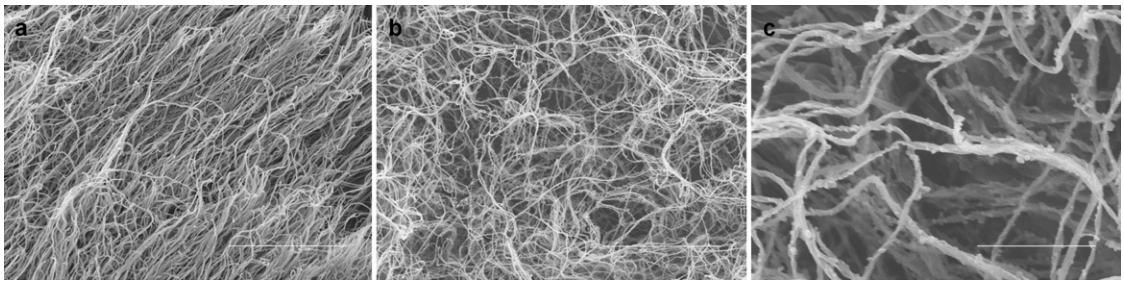

FIGURE 7 SEM images of gels formed at 37°C. (*a*) 0.5 mg/mL collagen at 4000× magnification, (*b*) 0.5 mg/mL collagen and 1.8 mg/mL HA at 4000× magnification, (*c*) 0.5 mg/mL collagen and 1.8 mg/mL HA at 20,000× magnification. Scale bar is 10 μm in *a* and *b* and 2 μm in *c*.

At equilibrium, the collagen/HA gels show slightly enhanced G'_∞ compared to pure collagen gels prepared under the same conditions (Table 1), consistent with the results of Hsu et al. (31). One possible explanation for the differences in G'_∞ between collagen and collagen/HA gels is that the dispersed HA itself forms a weak gel, adding extra rigidity to the matrix. Indeed, the difference in G'_∞ for the pure collagen gels and the collagen/HA gels is similar to the G'_∞ of cured pure HA ($G' \approx 0.1$ Pa for 2.0 mg/mL HA, data not shown). We also note that frequency sweeps of the equilibrium collagen/HA gels show greater frequency dependence (data not shown) than do those of pure collagen gels. Although there is almost no frequency dependence seen from 0.1–10.0 Hz for even the 0.5 mg/mL collagen gel, there is a noticeable increase in G' and G'' as a function of frequency in the collagen/HA gels. This is in agreement with the findings of Xin et al. (33). This is also consistent with the fact that the loss tangent is greater for collagen/HA gels than for collagen gels alone (Fig. 8). Thus, by certain measures HA weakens collagen gels formed at 37°C even as it increases their equilibrium storage moduli. All of these effects are seen most strongly in the 0.5 mg/mL collagen/HA gel, where the HA concentration is significantly greater than the collagen concentration.

Gelation dynamics

The effects of HA on the rate of gelation is investigated by rheology and CRM. Fig. 8 *a* shows rheology time sweeps of collagen/HA solutions at three concentrations. The basic shape of these curves is very similar to that of pure collagen solutions prepared at the same collagen concentration. The most obvious difference is in the increased initial G'' in the collagen/HA solutions. The increased value of the loss modulus also affects the value of the loss tangent during gelation. Fig. 8 *b* shows that the loss tangent of a 0.5 mg/mL collagen gel with HA is greater than that of the pure collagen gel both during gelation and at equilibrium. Comparison of G'_r for collagen and collagen/HA solutions shows a moderate increase in k_g with addition of HA (Table 1 and Fig. 8 *c*).

The sol-gel phase transitions of collagen/HA gels are studied rheologically in terms of t_c and t_g. The addition of HA to 0.5 mg/mL, 1.0 mg/mL, and 1.5 mg/mL collagen clearly increases t_c (Table 1). This is driven largely by the increased initial G'' of the collagen/HA solutions. We find t_c to vary more substantially as a function of frequency in collagen/HA systems than in pure collagen systems. Thus, although t_c is very close to t_g in the pure collagen systems, this is not the case in the collagen/HA systems. However, quantifying t_g is difficult in the collagen/HA systems, as a single tan δ crossing point does not always occur for the three frequencies probed. In Table 1, we thus report the point at which the 0.1- and 1-Hz measurements cross. Although t_c occurs significantly later and at higher G_c' in the presence of HA, t_g occurs only slightly later. The value of tan δ_g gives $\Delta \approx 0.7$ in the collagen/HA systems (Table 1). This value is close to theoretical predictions and to that found by Forgacs et al. (19) for the development of pure collagen gels at 12°C (19,60,61). However, given our previous discussion of t_g relative to the rise of G' and the fact that it is not possible to find a crossing point in all cases when plotting tan δ versus t, we suggest that t_g is not a clean measure of gelation in these complex physicochemical gels.

We further elucidate how HA affects collagen gelation kinetics via CRM (Movie S2 in the Supporting Material). We find that the addition of HA marginally shortens the time to arrest, t_a, for gels at each collagen concentration relative to gels without HA (Table 1). That this trend is not evident in t_c or t_g highlights the complementary nature of rheology and CRM for the study of gelation. The arrest time in CRM measures the immobilization of a developing 3D gel and relies on the interconnection of fibrils/fibers/clusters into a sample-spanning elastic network. The development of this network is affected by the viscosity of the background medium. For a given collagen concentration, the addition of HA increases the viscosity of the background. This is expected to slow the initial steps of gelation by decreasing the rate of monomer encounter and assembly into nuclei but may speed later portions of the gelation process by holding microstructures in place, thus facilitating fiber interconnection. As such, the presence of HA may shorten time to arrest even as it lengthens time to crossover, and we argue that although arrest time is a clear manifestation of the presence of a sample spanning network, the crossover time is not.

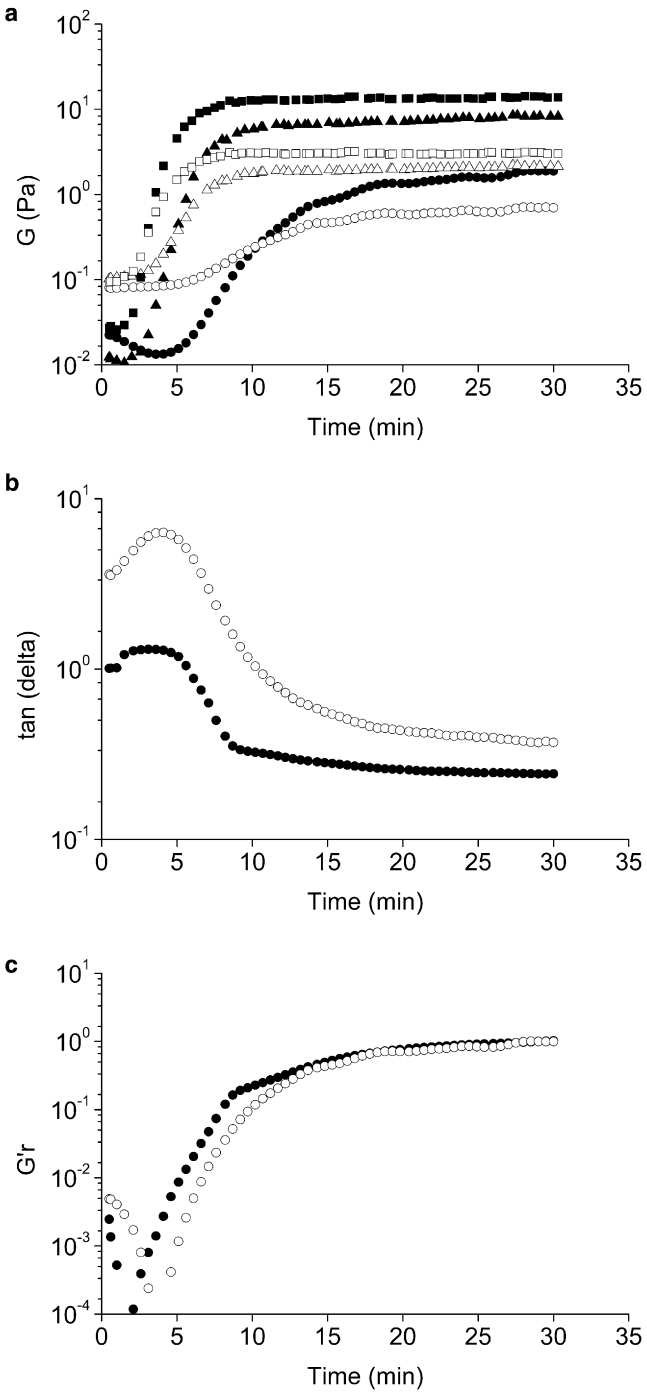

FIGURE 8 Gelation dynamics of collagen/HA gels at 37°C as measured by rheology. (*a*) Oscillatory time sweeps at 1 Hz during gelation. Solid symbols indicate storage modulus, G', and open symbols indicate loss modulus G''. Gels are 0.5 mg/mL collagen and 1.8 mg/mL HA (*circles*), 1.0 mg/mL collagen and 1.8 mg/mL HA (*triangles*), and 1.5 mg/mL collagen and 1.2 mg/mL HA (*squares*). (*b*) Loss tangent of the 0.5 mg/mL collagen gel (*solid symbols*) and the 0.5 mg/mL and 1.8 mg/mL HA (*open symbols*). (*c*) The reduced elastic modulus, G_r', for an 0.5 mg/mL collagen gel (*solid symbols*) and the 0.5 mg/mL and 1.8 mg/mL HA (*open symbols*).

As in pure collagen gels, the structures of collagen/HA systems at arrest mirror the structures at equilibrium, with more numerous, shorter, and thinner fibers in the presence of HA than in its absence. This can be seen in visual comparison of Figs. 4 and 9 (arrest) as well as Figs. 3 and 6 (equilibrium) (see Figs. 15 and 16 for summary). The presence of increased numbers of fibers during all stages of gelation implies the rate of formation of collagen nuclei is higher in the presence of HA. The modest increase in k_g then also suggests that these nuclei grow more quickly into fibrils in the presence of HA. The fact that more fibers are necessary to lead to arrest in the presence of HA is likely because the fibers in collagen/HA gels are thinner than those in pure collagen gels, suggesting that HA changes the shape of the forming nuclei. We propose that this occurs through dynamic, weak interactions of collagen with HA, the same interactions that result in the small proportion of deposited HA along the fibers in the equilibrium structure.

Collagen and collagen/HA matrices assembled at 32°C

Equilibrium

The temperature of gelation affects both dynamics of gelation and equilibrium structure and mechanical properties of collagen based gels. Fig. 10 shows that the same trends in equilibrium structure apparent at 37°C (Fig. 3) as a function of collagen concentration are also evident at 32°C. More numerous, shorter fibers are present as collagen concentration increases. However, a much stronger trend is evidenced as a function of temperature. All collagen gels formed at 32°C have fewer, longer, thicker fibers than do those formed at the same concentration at 37°C. This is consistent with a decrease in the nucleation rate with decreasing temperature. SEM measurements confirm that fibrils formed at 32°C are thicker than those formed at 37°C. Moreover, fibril thickness increases substantially as collagen concentration increases, unlike in gels formed at 37°C. This difference may be related to the fact that fibrillogenesis is slow enough at 32°C to allow for fuller development of the nuclei than at 37°C, where the onset of the growth phase occurs early in fibrillogenesis.

Differences between collagen and collagen/HA microstructures as measured by SEM are similar at 37°C (Fig. 7) and 32°C (Fig. 11). At 32°C, addition of HA leads to decreased fibril thickness and bundling as it does at 37°C. Moreover, CRM images show more and shorter fibers in the presence of HA (see Fig. 15). The most significant difference between collagen/HA gels at equilibrium formed at 32°C and at 37°C is illustrated by Fig. 12. Comparison of Figs. 5 and 12 reveals that the temperature of gelation changes the distribution of HA, and at 32°C more fluorescein-HA colocalizes with collagen fibers. The inset of Fig. 12 *b* shows a histogram of pixel intensities from CFM images of HA in collagen/HA gels formed at 37°C and 32°C. The substantial non-Gaussian tail present in the

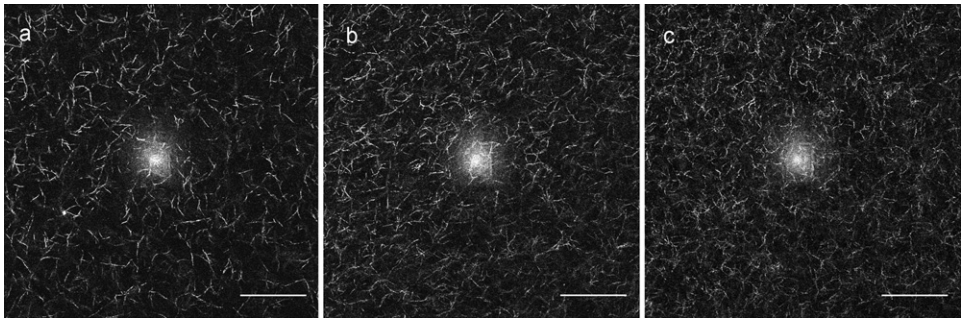

FIGURE 9 Confocal reflectance images of collagen/HA matrices recorded at the arrest time during gelation at 37°C: (*a*) 0.5 mg/mL collagen and 1.8 mg/mL HA, (*b*) 1.0 mg/mL collagen and 1.8 mg/mL HA, and (*c*) 1.5 mg/mL collagen and 1.2 mg/mL HA. Scale bar is 50 μm.

32°C gels is caused by the clustering of HA, clustering that is colocalized with collagen fibers. The different distributions of HA at 32°C and 37°C helps clarify the individual roles played by the dispersed and the deposited HA during gelation, as described below.

The equilibrium elastic moduli of all gels formed at 32°C are markedly increased relative to samples of the same composition gelled at 37°C (Tables 1 and 2). Although collagen gels with larger pore sizes generally are expected to have lower G'_∞, here any decrease in stiffness attributable to increase in mesh size appears to be more than offset by the increase in fibril thickness at the lower temperature. This is consistent with the fact that G'_∞ of these collagen gels increases more significantly as a function of concentration when gelled at 32°C than at 37°C, with $G'_\infty(c) \propto c^{2.6}$ at 32°C compared to $G'_\infty(c) \propto c^{2.1}$ at 37°C (Fig. 13 *a*). The fact that the scaling exponent varies with temperature is likely related to both overall gel structure and details of fiber structure. Mesh size decreases more substantially at 32°C than at 37°C, and fibrils become substantially thicker at 32°C over this concentration range (Fig. 13 *a*). Moreover, differences in collagen monomer triple helical character at these two temperatures may change the relative distribution of crosslinks and entanglements in networks formed at these temperatures (63). We also note that collagen samples with HA again show moderate increases in G'_∞ compared to pure collagen when gelled at 32°C (Table 2). As at 37°C, we suggest the dispersed HA is mostly responsible for this change.

Gelation dynamics

The gelation dynamics at 32°C is first evaluated via rheology. Fig. 13, *b* and *c*, reveals that the full gelation process is

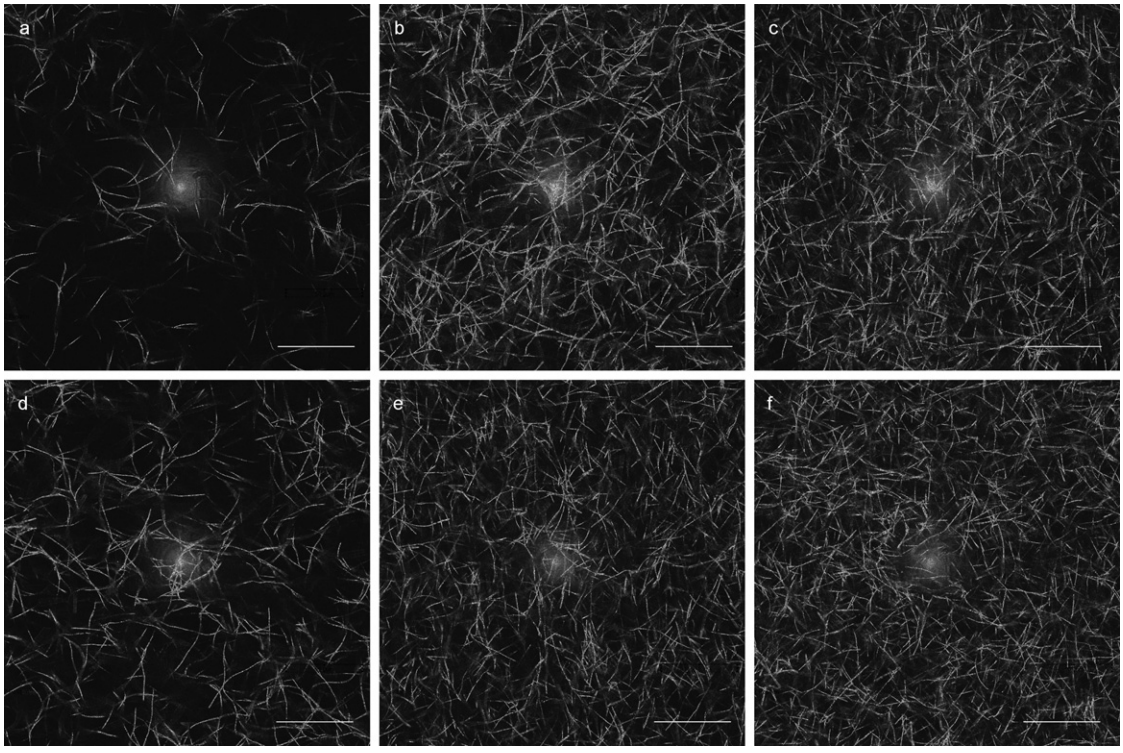

FIGURE 10 Confocal reflectance images of gels recorded at equilibrium after gelation at 32°C: (*a*) 0.5 mg/mL collagen, (*b*) 1.0 mg/mL collagen, (*c*) 1.5 mg/mL collagen, (*d*) 0.5 mg/mL collagen and 1.8 mg/mL HA, (*e*) 1.0 mg/mL collagen and 1.8 mg/mL HA, and (*f*) 1.5 mg/mL collagen and 1.2 mg/mL HA. Scale bar is 50 μm.

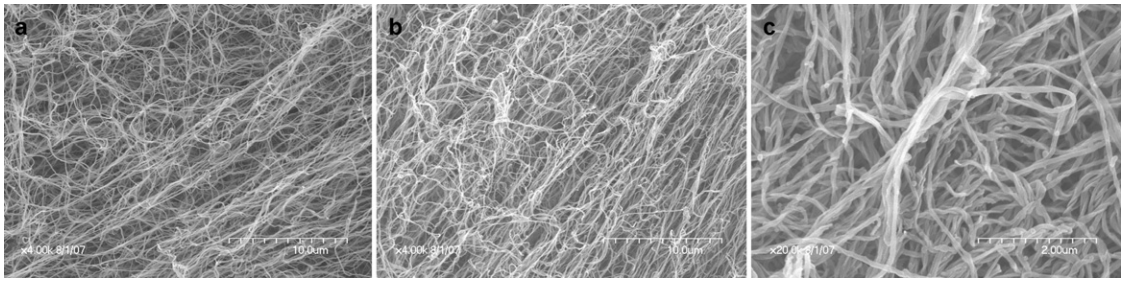

FIGURE 11 SEM images of gels formed at 32°C: (*a*) 0.5 mg/mL collagen at 4000× magnification, (*b*) 0.5 mg/mL collagen and 1.8 mg/mL HA at 4000× magnification, and (*c*) 0.5 mg/mL collagen and 1.8 mg/mL HA at 20,000× magnification. Scale bar is 10 μm in *a* and *b* and 2 μm in *c*.

substantially slower at 32°C than at 37°C, as illustrated by the longer time required to reach the equilibrium values of G' and G'' at all concentrations. Fig. 13 also shows that the shape of the pure collagen (Fig. 13 *b*) and collagen/HA (Fig. 13 *c*) time sweep curves differ from those at 37°C. The plots in Fig. 13 show a two-step increase in G'. The first increase is very short (~2 min for 1.5 mg/mL collagen and ~4 min for 0.5 mg/mL collagen) and followed by a long period during which the storage modulus rises very slowly (~5 min for 1.5 mg/mL collagen and ~13 min for 0.5 mg/mL collagen). This is followed by a second, more obvious, increase in G'. Given the shape of these curves relative to those at 37°C as well as to CRM measurements described below, we consider the lag time t_{lag} here to be the time before the onset of the first increase in G' and k_g to be represented by the second increase in G'. At 32°C, because the nuclei are larger and sparser and transport of molecules is slower than at 37°C, fiber lengthening occurs largely before fiber entanglement. We believe the formation of effective interconnections is responsible for the second, more substantial, increase in G'.

Because of the different shape of the time sweep rheology curves at 37°C and 32°C, there is difficulty directly

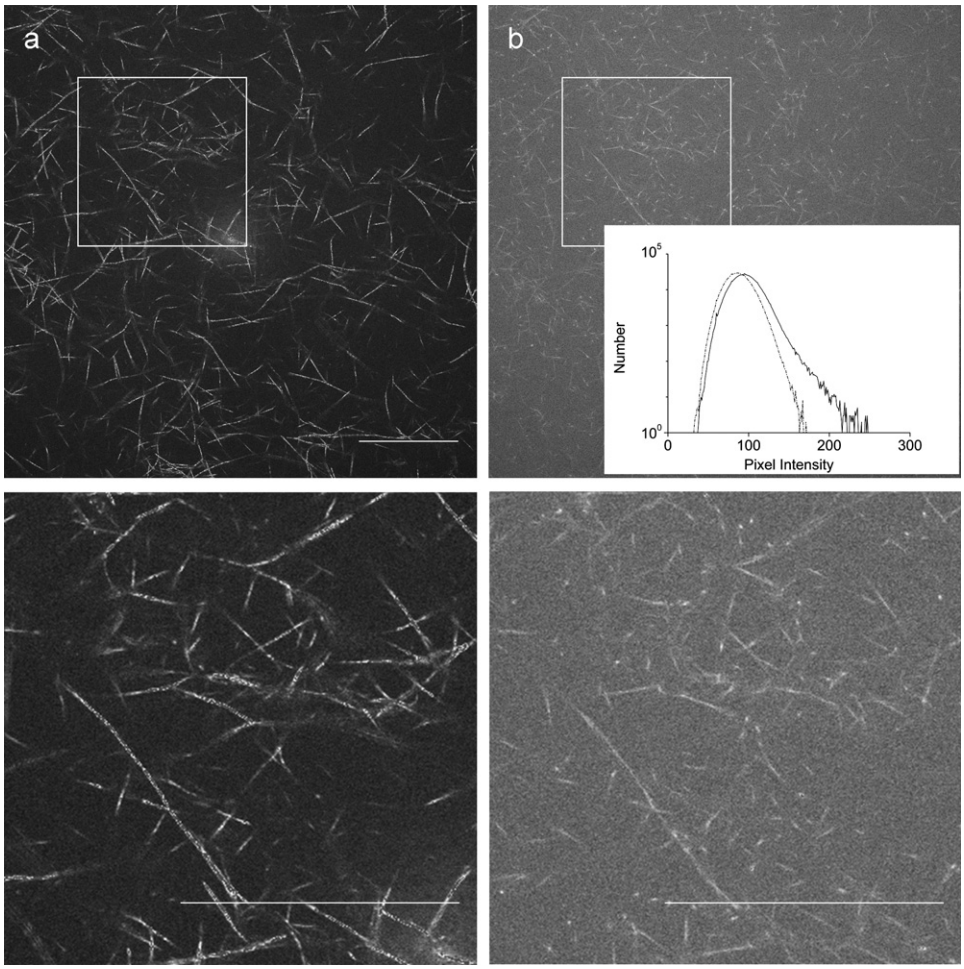

FIGURE 12 Consecutively collected (*a*) CRM and (*b*) CFM images of a 1.0 mg/mL collagen gel containing 1.8 mg/mL fluorescein-labeled HA gelled at 32°C. Lower panel shows close-ups of the squared portions of images in the upper panel. Scale bar is 50 μm. Inset shows summed histograms of pixel intensities of two CFM images of HA at 32°C (*solid*) and 37°C (*dashed*). The substantial non-Gaussian tail for images of gels formed at 32°C is caused by clusters of HA, which colocalize with collagen.

TABLE 2 Measures of collagen and collagen/HA mechanical properties, structure, and gelation dynamics at 32°C*

		Equilibrium	Dynamics		
			Gelation rate	Sol-gel transition	CRM
Collagen (mg/mL)	HA (mg/mL)	G'_∞ (Pa)	k_{growth} (min^{-1} ± SD)	t_c (min ± SD)	t_a (min ± SD)
0.5	0	1.77 ± 0.06	0.049 ± 0.003	(19 ± 1)	13.0 ± 0.9
1.0	0	11.5 ± 0.4	0.10 ± 0.01	(16.3 ± 0.8)	13 ± 2
1.5	0	29.5 ± 0.4	0.23 ± 0.04	(7.9 ± 0.6)	9 ± 2
0.5	1.8	2.33 ± 0.05	0.066 ± 0.003	24.5 ± 0.8	23 ± 3
1.0	1.8	14.1 ± 0.6	0.124 ± 0.009	21 ± 1	17 ± 1
1.5	1.2	30.6 ± 0.9	0.22 ± 0.04	11 ± 2	12 ± 4

Measures of mechanical properties (G'_∞), kinetics of gelation (k_g), and sol-gel transition (t_c, t_a) for networks constructed at 32°C as described in the text. All measures are determined as described in the caption of Table 1. In the pure collagen gels, there is no crossover time in the rapidly increasing region of G', and thus, the time at which G' and G'' come nearest each other is reported instead. These measurements are presented in parentheses.

comparing t_{lag} and k_g at these two temperatures. There is also difficulty comparing the sol-gel transition as measured via rheology. Indeed, crossover occurs very early in the gelation time sweep of pure collagen solutions. This time is earlier than t_c at 37°C and is a time in which very few if any fibers are visible via CRM. Thus, this early t_c is not descriptive of the system containing a structure that is spanning or nearly spanning. Instead, we define t_c as the time of nearest approach of G' and G'' during the second increase in G' (Table 2). Because of the lack of a true crossover time here, it is not possible to identify t_g, again suggesting that t_g is not a clear descriptor of the sol-gel transition in this complex physicochemical gel. Regardless of these complications, if we consider t_{lag}, k_g, and t_c (as well as the time required to reach G'_∞) as described above, it is clear that gelation at 32°C is slower than at 37°C and that trends as a function of concentration are the same at 37°C and 32°C: t_{lag} decreases, k_g increases, and t_c decreases.

Although the time sweep rheology changes substantially with gelation temperature, the dynamics of the process looks fairly similar at 37°C and 32°C as measured by CRM. This is largely because the most significant differences in rheology occur at very early times, before structures visualizable in CRM are formed. At 32°C the same trends visible as a function of concentration at equilibrium are also apparent at arrest (Fig. 14). More fibers are present as concentration increases, although fibers are fewer and longer than at the same concentration at 37°C (see Fig. 16). The arrest time, t_a, also decreases as concentration increases, as at 37°C. Because it is unclear how t_c and t_g relate to the sol-gel transition in collagen gelation at 32°C for the reasons described above, t_a is the only straightforward descriptor of gelation we measure for fibrillogeneisis at 32°C.

Although most trends seen at 37°C are also seen at 32°C, there are some differences. As at 37°C, addition of HA leads to the presence of increased numbers of fibers and decreased mesh size at both equilibrium and arrest (Figs. 15 and 16). Similarly, HA moderately increases k_g and more obviously increases t_c at 32°C, as at 37°C (Tables 1 and 2). The increase in t_c is driven by the increased viscosity of the background solution in the presence of HA. However, unlike at 37°C, t_a clearly becomes later with the addition of HA at 32°C. We speculate that this is driven by the same differences in gelation dynamics at the two temperatures that result in the different distributions of HA at the two temperatures (Figs. 5 and 12). At 37°C, short and thin fibrils assemble very quickly around dense structured centers. Deposition of HA on fibrils that may bundle into fibers during such fast gelation is not very effective, and a large amount of HA remains dispersed in the gel. At 32°C, long and thick fibers slowly assemble around fewer structured centers. During this slower assembly process, a significant amount of HA deposits along fibrils, and fewer HA molecules remain dispersed in the medium. At 37°C, the dispersed HA adds sufficient viscosity in the background to hold the forming fibrils and fibers together, and this marginally decreases the time to arrest. This occurs although some HA is dynamically interacting with the collagen molecules as they form nuclei and fibrils, reducing fibril diameter and bundling. Unlike at 37°C, at 32°C there may not be sufficient HA dispersed in the background to stabilize the collagen/HA gels against the effects of decreased fibril width and bundling, resulting in the delayed arrest time. At both temperatures, more fibers are necessary to achieve a stable network at arrest in the presence of HA, as is seen in Fig. 16 *b*. At 37°C these more numerous fibers appear on a very similar timescale to the slightly longer, thicker fibers that form in that system without HA, implying that the nucleation rate is increased in the presence of HA. The increased nucleation rate does not appear to occur at 32°C; fewer fibers are present at the same times in the presence of HA relative to in its absence (data not shown). This is consistent with the fact that the slowly assembling collagen molecules interact more substantially with HA at 32°C than at 37°C, both slowing the overall fibrillogenesis and resulting in increased deposited HA. The arrest cannot occur until the nucleated fibrils assemble substantially, and the arrest time is significantly delayed in the presence of HA compared to that in pure collagen gels. Together with results at 37°C, it can be concluded that the arrest time t_a is affected by both the dispersed HA and the deposited HA. The former factor dominates at 37°C, and the latter factor dominates at 32°C.

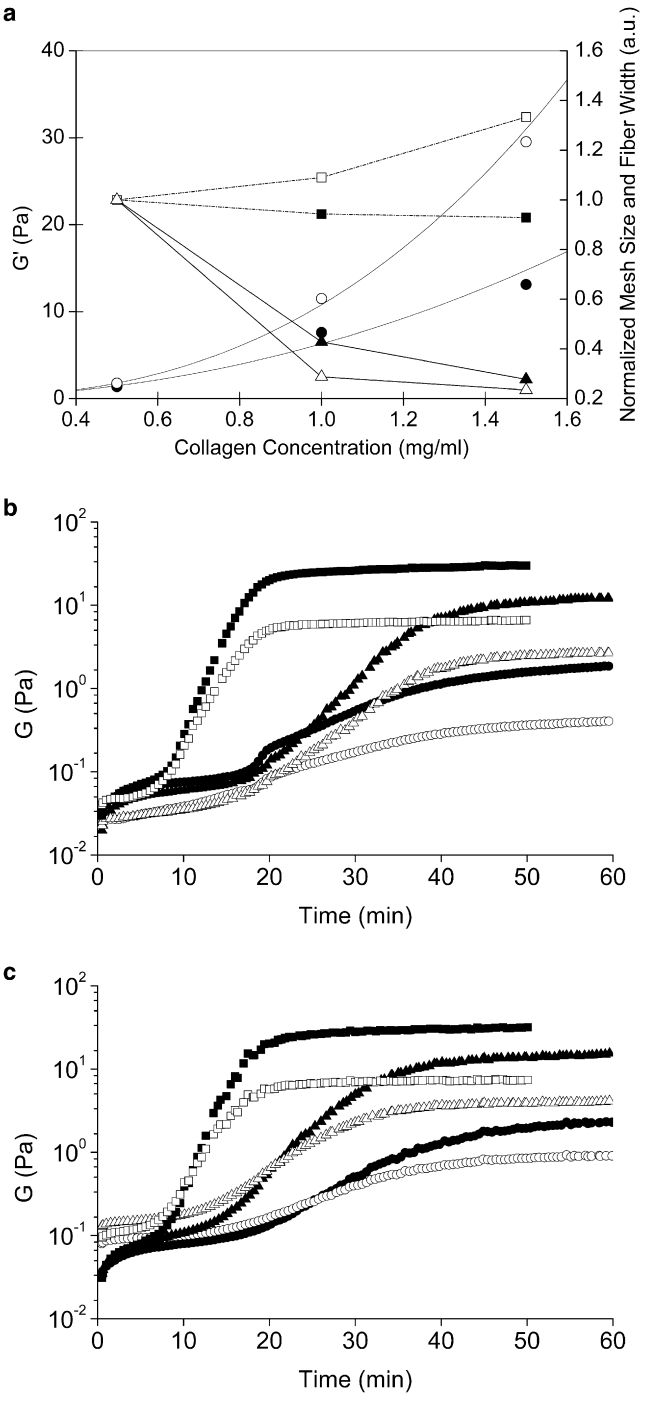

FIGURE 13 (*a*) Elastic modulus (*left axis*) of collagen gels at 32°C (*open circles*) and 37°C (*solid circles*). Lines are the functions $G'(c) = 10.8c^{2.6}$ and $G'(c) = 6.3c^{2.1}$, respectively. Mesh size (*triangles, dashed lines*) and fiber width (*squares, dotted lines*) at equilibrium are shown on the right axis. Open symbols are for gels formed at 32°C, and solid symbols are for those formed at 37°C. Gelation dynamics of (*b*) collagen and (*c*) collagen/HA gels at 32°C as measured by rheology. Oscillatory time sweeps at 1 Hz during gelation. Solid symbols indicate storage modulus, G', and open symbols indicate loss modulus G''. In *b*, collagen concentrations are 0.5 (*circles*), 1.0 (*triangles*), and 1.5 mg/mL (*squares*). In *c*, concentrations are 0.5 mg/mL collagen and 1.8 mg/mL HA (*circles*), 1.0 mg/mL collagen and 1.8 mg/mL HA (*triangles*), and 1.5 mg/mL collagen and 1.2 mg/mL collagen (*squares*).

CONCLUSION

In this work, the equilibrium properties and dynamic fibrillogenesis of collagen and collagen/HA gels were studied chiefly by the complementary techniques of rheology and CRM. Rheological measurements monitor the buildup of mechanical properties of these gels, whereas time-lapse CRM directly monitors microstructural development responsible for the overall mechanical behavior during gelation. The dual use of these techniques thus provides unique insight into how structures that arise during fibrillogenesis affect the viscoelasticity of the system, an important consideration both for biophysical studies and bioengineering applications. Below, we summarize some of the major findings of this work.

At equilibrium, large changes in fiber number and mesh size and small changes in fiber length and width are found to occur with concentration over the range of 0.5 to 1.5 mg/mL collagen at both 37°C and 32°C. On the other hand, both network and fiber structure are found to vary strongly with gelation temperature, with fewer, longer, and thicker fibers present at 32°C than 37°C, in accord with nucleation and growth theory. The equilibrium elastic moduli are higher in all cases at 32°C despite the greater pore size in these systems, suggesting that fibril thickness is more important than pore size in setting the value of G'_∞ in this range of pore size and fiber thickness. G'_∞ also scales more strongly with concentration at 32°C than at 37°C as a result of differences in both network and fiber structure at these temperatures. The presence of HA increases fiber number, decreases fibril diameter, and slightly increases G'_∞ of all systems investigated. As revealed by CFM and SEM, HA in collagen/HA gels can both deposit on collagen fibrils and disperse throughout the medium. The distribution of HA changes with temperature, and when the temperature decreases from 37°C to 32°C, more HA is deposited on collagen fibrils.

The dynamics of collagen and of collagen/HA gelation at 37°C and 32°C were also investigated via time-sweep rheology and time-lapse CRM in this work, and each technique yields a wealth of new information. For example, whereas a previous study of collagen gelation found that percolation theory accounted for several crucial aspects of the rheological behavior of collagen gels formed at low temperatures, our results show this is not the case at more physiologically relevant temperatures. We find that, at 37°C, the exponent Δ is significantly smaller than that predicted by percolation theory. At 32°C, we cannot define t_g, a frequency-independent measure of gelation, again inconsistent with percolation theory. Using CRM to monitor microstructure during gelation provides an alternate way to interrogate and describe the gelation time in these systems by directly identifying the time, t_a, at which the network spans the sample. In particular, we find that in all cases, structural trends as a function of gel composition and gelation temperature evident at equilibrium are also apparent at the arrest time, t_a, consistent with predictions of the nucleation and growth

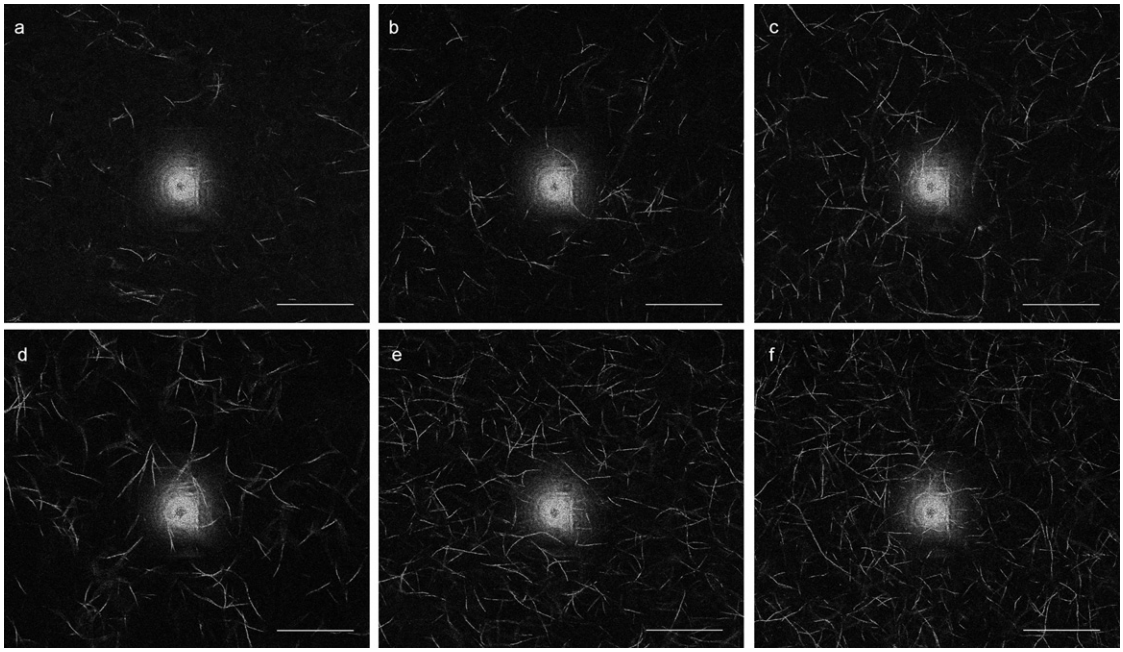

FIGURE 14 Confocal reflectance images of gels recorded at the arrest time during gelation at 32°C: (*a*) 0.5 mg/mL collagen, (*b*) 1.0 mg/mL collagen (*c*) 1.5 mg/mL collagen, (*d*) 0.5 mg/mL collagen and 1.8 mg/mL HA, (*e*) 1.0 mg/ml collagen and 1.8 mg/ml HA, and (*f*) 1.5 mg/mL collagen and 1.2 mg/mL HA. Scale bar is 50 *u*m.

model of collagen gelation. Addition of HA is found to have different effects at 37°C and 32°C, which is in part a cause and in part a result of the different distributions of HA in the collagen gels at these two temperatures.

Complementary investigation of the structural and mechanical properties of developing biopolymer networks, as has been performed in this study, opens up new avenues for gaining precise microscopic understanding of these complex gelation processes. Such investigation will allow for enhanced rational design of biomaterials of particular structure, mechanical properties, and composition for use in biophysical studies and bioengineering applications. Moreover, studies detailing how structure imparts mechanical properties in dynamic biopolymer networks will allow fuller understanding of important physiological processes. Such processes may extend beyond in vivo formation of ECM to aspects of the formation and remodeling of the highly dynamic cytoskeletal network.

SUPPORTING MATERIAL

Two movies are available at http://www.biophysj.org/biophysj/supplemental/S0006-3495(08)03224-4.

L.J.K. thanks David Vader, Andy Stein, Cheng Guo, and David Reichman for helpful discussions.

L.J.K. acknowledges the support of the NYSTAR James D. Watson and the Beckman Young Investigator Awards.

REFERENCES

1. Comper, W. D. 1996. Extracellular Matrix. Harwood Academic Publishers, Amsterdam.
2. Alberts, B. 2002. Molecular Biology of the Cell. Garland Science, New York.
3. Scott, J. E. 1988. Proteoglycan-fibrillar collagen interactions. *Biochem. J.* 252:313–323.
4. Laurent, T. C., and J. R. Fraser. 1992. Hyaluronan. *FASEB J.* 6: 2397–2404.
5. Laurent, T. C. 1998. Chemistry and Biology and Medical Applications of Hyaluronan and its Derivatives. Portland Press, London.
6. Salomone, J. C. 1996. Polymeric Materials Encyclopedia. CRC Press, Boca Raton, FL.
7. Mow, V. C., M. H. Holmes, and W. M. Lai. 1984. Fluid transport and mechanical properties of articular cartilage: A review. *J. Biomech.* 17:377–394.
8. Toole, B. P. 2004. Hyaluronan: From extracellular glue to pericellular cue. *Nat. Rev. Cancer.* 4:528–539.
9. Wood, G. C., and M. K. Keech. 1960. The formation of fibrils from collagen solutions. 1. The effect of experimental conditions: Kinetic and electron-microscope studies. *Biochem. J.* 75:588–598.
10. Wood, G. C. 1960. The formation of fibrils from collagen solutions. 2. A mechanism of collagen-fibril formation. *Biochem. J.* 75:598–605.
11. Comper, W. D., and A. Veis. 1977. Characterization of nuclei in *in vitro* collagen fibril formation. *Biopolymers.* 16:2133–2142.
12. Comper, W. D., and A. Veis. 1977. The mechanism of nucleation for *in vitro* collagen fibril formation. *Biopolymers.* 16:2113–2131.
13. Williams, B. R., R. A. Gelman, D. C. Poppke, and K. A. Piez. 1978. Collagen fibril formation. Optimal in vitro conditions and preliminary kinetic results. *J. Biol. Chem.* 253:6578–6585.
14. Silver, F. H., and D. E. Birk. 1983. Kinetic-analysis of collagen fibrillogenesis. 1. Use of turbidity–time data. *Coll. Relat. Res.* 3: 393–405.
15. Na, G. C., L. J. Butz, and R. J. Carroll. 1986. Mechanism of *in vitro* collagen fibril assembly. Kinetic and morphological studies. *J. Biol. Chem.* 261:12290–12299.
16. Holmes, D. F., R. B. Watson, and K. E. Kadler. 1991. On the regulation of collagen-fibril shape and form. *Biochem. Soc. Trans.* 19:808–811.

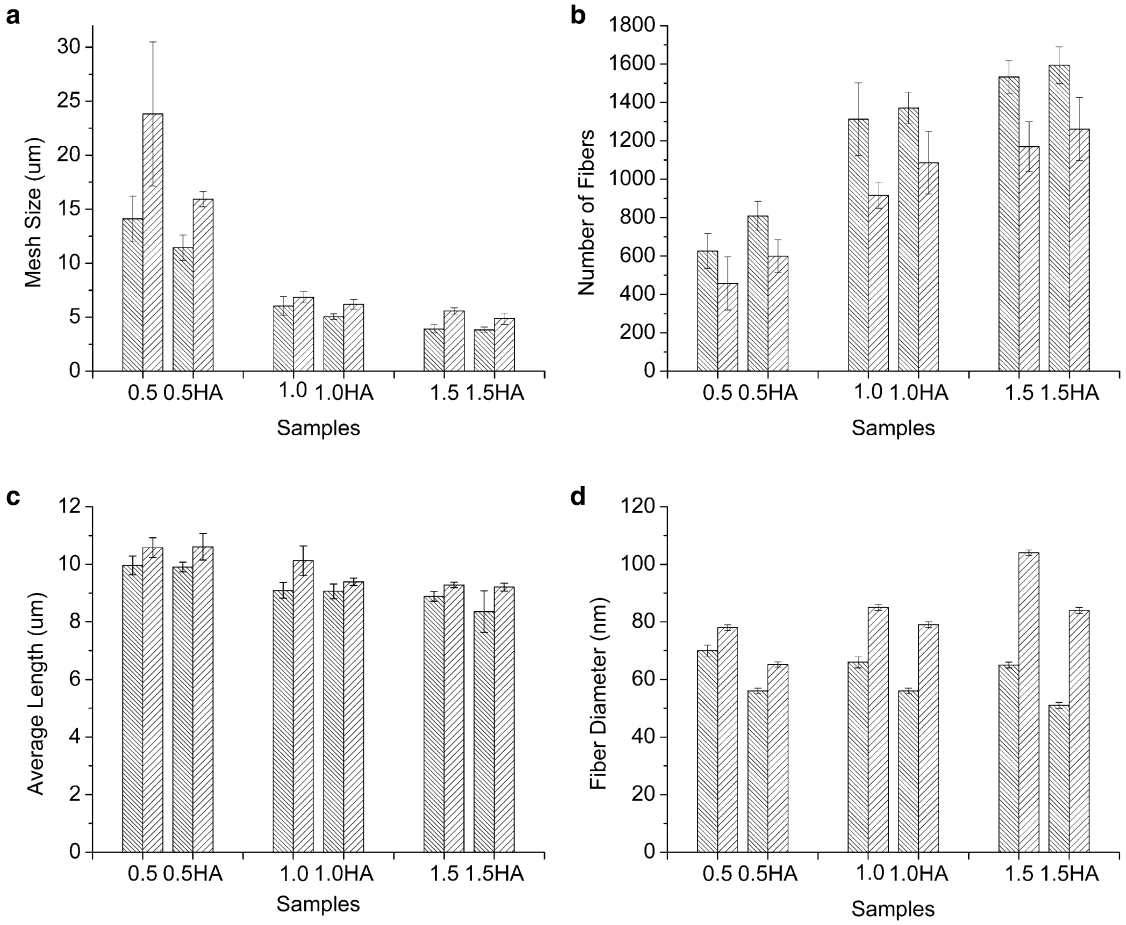

FIGURE 15 Summary of equilibrium values of (*a*) mesh size, (*b*) fiber number, (*c*) fiber length, and (*d*) fibril diameter as described in the text. Average is over four samples, and error bar is standard deviation. Samples are 0.5 mg/mL collagen (0.5); 0.5 mg/mL collagen and 1.8 mg/mL HA (0.5HA); 1.0 mg/mL collagen (1.0); 1.0 mg/mL collagen and 1.8 mg/mL HA (1.0HA); 1.5 mg/mL collagen (1.5); 1.5 mg/mL collagen and 1.2 mg/mL HA (1.5HA). Data at 37°C are represented by dense diagonal lines that run from upper left to lower right, and data at 32°C by sparser diagonal lines that run from lower left to upper right.

17. Kadler, K. E., D. F. Holmes, J. A. Trotter, and J. A. Chapman. 1996. Collagen fibril formation. *Biochem. J.* 316:1–11.
18. Brightman, A. O., B. P. Rajwa, J. E. Sturgis, M. E. McCallister, J. P. Robinson, et al. 2000. Time-lapse confocal reflection microscopy of collagen fibrillogenesis and extracellular matrix assembly in vitro. *Biopolymers.* 54:222–234.
19. Forgacs, G., S. A. Newman, B. Hinner, C. W. Maier, and E. Sackmann. 2003. Assembly of collagen matrices as a phase transition revealed by structural and rheologic studies. *Biophys. J.* 84:1272–1280.
20. Christiansen, D. L., E. K. Huang, and F. H. Silver. 2000. Assembly of type I collagen: Fusion of fibril subunits and the influence of fibril diameter on mechanical properties. *Matrix Biol.* 19:409–420.
21. Silver, F. H., J. W. Freeman, and G. P. Seehra. 2003. Collagen self-assembly and the development of tendon mechanical properties. *J. Biomech.* 36:1529–1553.
22. Durand, D., M. Delsanti, M. Adam, and J. M. Luck. 1987. Frequency-dependence of viscoelastic properties of branched polymers near gelation threshold. *Europhys. Lett.* 3:297–301.
23. De Gennes, P. G. 1988. Scaling Concepts in Polymer Physics. Cornell University Press, Ithaca, NY.
24. Clerc, J. P., G. Giraud, J. M. Laugier, and J. M. Luck. 1990. The AC electrical-conductivity of binary disordered-systems, percolation clusters, fractals and related models. *Adv. Phys.* 39:191–308.
25. Stauffer, D., and A. Aharony. 1992. Introduction to Percolation Theory. Taylor and Francis, London.
26. Sahimi, M. 1994. Applications of Percolation Theory. Taylor and Francis, London.
27. Wood, G. C. 1960. The formation of fibrils from collagen solutions. 3. Effect of chondroitin sulphate and some other naturally occurring polyanions on the rate of formation. *Biochem. J.* 75:605–612.
28. Toole, B. P., and D. A. Lowther. 1968. Effect of chondroitin sulphate--protein on formation of collagen fibrils *in vitro*. *Biochem. J.* 109: 857–866.
29. Obrink, B. 1973. A study of the interactions between monomeric tropocollagen and glycosaminoglycans. *Eur. J. Biochem.* 33:387–400.
30. Turley, E. A., C. A. Erickson, and R. P. Tucker. 1985. The retention and ultrastructural appearances of various extracellular matrix molecules incorporated into three-dimensional hydrated collagen lattices. *Dev. Biol.* 109:347–369.
31. Hsu, S., A. M. Jamieson, and J. Blackwell. 1994. Viscoelastic studies of extracellular-matrix interactions in a model native collagen gel system. *Biorheology.* 31:21–36.
32. Salchert, K., U. Streller, T. Pompe, N. Herold, M. Grimmer, et al. 2004. In vitro reconstitution of fibrillar collagen type I assemblies at reactive polymer surfaces. *Biomacromolecules.* 5:1340–1350.

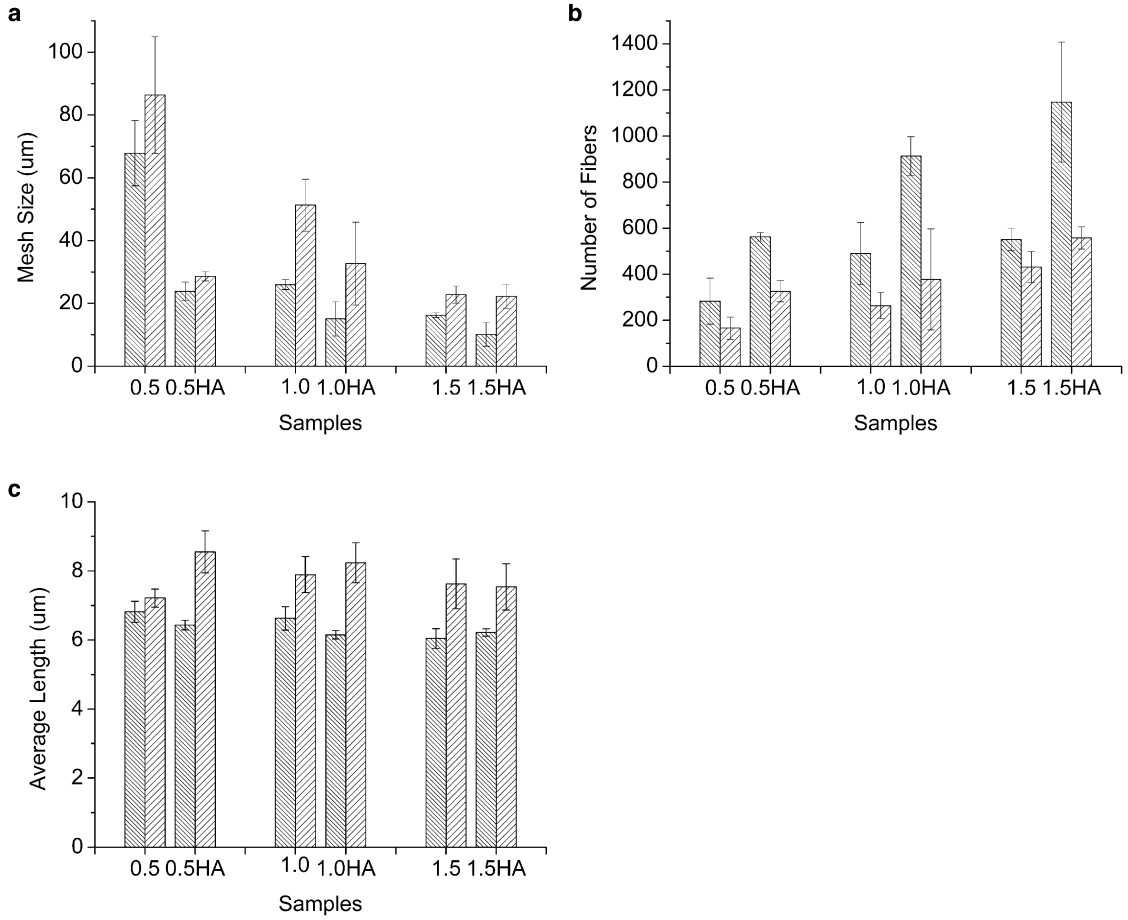

FIGURE 16 Summary of arrest values of (*a*) mesh size, (*b*) fiber number, and (*c*) fiber length as described in the text. Average is over three samples, and error bar is standard deviation. Samples are 0.5 mg/mL collagen (0.5); 0.5 mg/mL collagen and 1.8 mg/mL HA (0.5HA); 1.0 mg/mL collagen (1.0); 1.0 mg/mL collagen and 1.8 mg/mL HA (1.0HA); 1.5 mg/mL collagen (1.5); and 1.5 mg/mL collagen and 1.2 mg/mL HA (1.5HA). Data at 37°C are represented by dense diagonal lines that run from upper left to lower right, and data at 32°C by sparser diagonal lines that run from lower left to upper right.

33. Xin, X., A. Borzacchiello, P. A. Netti, L. Ambrosio, and L. Nicolais. 2004. Hyaluronic-acid-based semi-interpenetrating materials. *J. Biomater. Sci. Polym. Ed.* 15:1223–1236.
34. Tsai, S. W., R. L. Liu, F. Y. Hsu, and C. C. Chen. 2006. A study of the influence of polysaccharides on collagen self-assembly: Nanostructure and kinetics. *Biopolymers.* 83:381–388.
35. Raspanti, M., M. Viola, M. Sonaggere, M. E. Tira, and R. Tenni. 2007. Collagen fibril structure is affected by collagen concentration and decorin. *Biomacromolecules.* 8:2087–2091.
36. Erikson, A., H. N. Andersen, S. N. Naess, P. Sikorski, and C. D. Davies. 2008. Physical and chemical modifications of collagen gels: Impact on diffusion. *Biopolymers.* 89:135–143.
37. Stamov, D., M. Grimmer, K. Salchert, T. Pompe, and C. Werner. 2008. Heparin intercalation into reconstituted collagen I fibrils: Impact on growth kinetics and morphology. *Biomaterials.* 29:1–14.
38. Friedl, P., and E. B. Brocker. 2000. The biology of cell locomotion within three-dimensional extracellular matrix. *Cell. Mol. Life Sci.* 57:41–64.
39. Kaufman, L. J., C. P. Brangwynne, K. E. Kasza, E. Filippidi, V. D. Gordon, et al. 2005. Glioma expansion in collagen Ii matrices: Analyzing collagen concentration-dependent growth and motility patterns. *Biophys. J.* 89:635–650.
40. Wolf, K., Y. I. Wu, Y. Liu, J. Geiger, E. Tam, et al. 2007. Multi-step pericellular proteolysis controls the transition from individual to collective cancer cell invasion. *Nat. Cell Biol.* 9:893–904.
41. Purecol info centre, http://www.Purecol.Nu/.
42. Paddock, S. 2002. Confocal reflection microscopy: The "other" confocal mode. *Biotechniques.* 32:274–277.
43. Guo, C., and L. J. Kaufman. 2007. Flow and magnetic field induced collagen alignment. *Biomaterials.* 28:1105–1114.
44. Chiang-Ying, M. T., and P. J. Dynes. 1982. Relationship between viscoelastic properties and gelation in thermosetting systems. *J. Appl. Polym. Sci.* 27:569–574.
45. Winter, H. H., and F. Chambon. 1986. Analysis of linear viscoelasticity of a cross-linking polymer at the gel point. *J. Rheology.* 30:367–382.
46. Rosenblatt, J., B. Devereux, and D. G. Wallace. 1994. Injectable collagen as a pH-sensitive hydrogel. *Biomaterials.* 15:985–995.
47. Velegol, D., and F. Lanni. 2001. Cell traction forces on soft biomaterials. I. Microrheology of type I collagen gels. *Biophys. J.* 81: 1786–1792.
48. Chambon, F., and H. H. Winter. 1987. Linear viscoelasticity at the gel point of a crosslinking pdms with imbalanced stoichiometry. *J. Rheology.* 31:683–697.
49. Winter, H. H., P. Morganelli, and F. Chambon. 1988. Stoichiometry effects on rheology of model polyurethanes at the gel point. *Macromolecules.* 21:532–535.

50. Scanlan, J. C., and H. H. Winter. 1991. Composition dependence of the viscoelasticity of end-linked poly(dimethylsiloxane) at the gel point. *Macromolecules*. 24:47–54.

51. Djabourov, M., J. Leblond, and P. Papon. 1988. Gelation of aqueous gelatin solutions. 2. Rheology of the sol-gel transition. *J. Phys.* 49:333–343.

52. Nijenhuis, K. T., and H. H. Winter. 1989. Mechanical-properties at the gel point of a crystallizing poly(vinyl-chloride) solution. *Macromolecules*. 22:411–414.

53. Lin, Y. G., D. T. Mallin, J. C. W. Chien, and H. H. Winter. 1991. Dynamic mechanical measurement of crystallization-induced gelation in thermoplastic elastomeric poly(propylene). *Macromolecules*. 24:850–854.

54. Richtering, H. W., K. D. Gagnon, R. W. Lenz, R. C. Fuller, and H. H. Winter. 1992. Physical gelation of a bacterial thermoplastic elastomer. *Macromolecules*. 25:2429–2433.

55. Ponton, A., P. Griesmar, S. Barboux-Doeuff, and C. Sanchez. 2001. Rheological investigation of the sol–gel transition: Effect of hydrolysis variation in silicon oxide and titanium oxide based matrices. *J. Mater. Chem.* 11:3125–3129.

56. Ikeda, S., and K. Nishinari. 2001. Structural changes during heat-induced gelation of globular protein dispersions. *Biopolymers*. 59: 87–102.

57. Sahiner, N., M. Singh, D. D. Kee, V. T. John, and G. L. McPherson. 2006. Rheological characterization of a charged cationic network across the gelation boundary. *Polymer (Guildf.)*. 47:1124–1131.

58. Richter, S. 2007. Recent gelation studies on irreversible and reversible systems with dynamic light scattering and rheology - a concise summary. *Macromol. Chem. Phys.* 208:1495–1502.

59. Stauffer, D., A. Coniglio, and M. Adam. 1982. Gelation and critical phenomena. *Adv. Polym. Sci.* 44:103–158.

60. Adolf, D., J. E. Martin, and J. P. Wilcoxon. 1990. Evolution of structure and viscoelasticity in an epoxy near the sol-gel transition. *Macromolecules*. 23:527–531.

61. Yu, J. M., P. Dubois, P. Teyssie, R. Jerome, S. Blacher, et al. 1996. Triblock copolymer based thermoreversible gels. 2. Analysis of the sol-gel transition. *Macromolecules*. 29:5384–5391.

62. Muthukumar, M. 1989. Screening effect on viscoelasticity near the gel point. *Macromolecules*. 22:4656–4658.

63. Leikina, E., M. V. Mertts, N. Kuznetsova, and S. Leikin. 2002. Type I collagen is thermally unstable at body temperature. *Proc. Natl. Acad. Sci. USA*. 99:1314–1318.

64. Chandrakasan, G., D. A. Torchia, and K. A. Piez. 1976. Preparation of intact monomeric collagen from rat tail tendon and skin and structure of nonhelical ends in solution. *J. Biol. Chem.* 251:6062–6067.

65. Gelman, R. A., D. C. Poppke, and K. A. Piez. 1979. Collagen fibril formation *in vitro*—role of the non-helical terminal regions. *J. Biol. Chem.* 254:1741–1745.

66. Kuznetsova, N., and S. Leikin. 1999. Does the triple helical domain of type I collagen encode molecular recognition and fiber assembly while telopeptides serve as catalytic domains? Effect of proteolytic cleavage on fibrillogenesis and on collagen-collagen interaction in fibers. *J. Biol. Chem.* 274:36083–36088.

67. Raub, C. B., V. Suresh, T. Krasieva, J. Lyubovitsky, J. D. Mih, et al. 2007. Noninvasive assessment of collagen gel microstructure and mechanics using multiphoton microscopy. *Biophys. J.* 92:2212–2222.

68. Roeder, B. A., K. Kokini, J. E. Sturgis, J. P. Robinson, and S. L. Voytik-Harbin. 2002. Tensile mechanical properties of three-dimensional type I collagen extracellular matrices with varied microstructure. *J. Biomech. Eng.* 124:214–222.

69. Stein, A. M., D. A. Vader, D. A. Weitz, and L. M. Sander. 2008. The micromechanics of three dimensional collagen-I gels. *arXiv:0807.2805v1*.

70. Newman, S., M. Cloitre, C. Allain, G. Forgacs, and D. Beysens. 1997. Viscosity and elasticity during collagen assembly *in vitro*: Relevance to matrix-driven translocation. *Biopolymers*. 41:337–347.

71. Rosa, E. D., C. Borselli, and P. A. Netti. 2006. Transport of large molecules in hyaluronic acid-based membranes and solution. *J. Membr. Sci.* 273:84–88.